Methods for
Ionization Current Interpretation
to be Used in Ignition Control

Lars Eriksson

Methods for
Ionization Current Interpretation
to be Used in Ignition Control

Examensarbete utfört i Fordonssystem
vid Tekniska Högskolan i Linköping
av

Lars Eriksson

Reg nr: LiTH-ISY-EX-1507

Supervisor: **Jan Nytomt**
Lars Nielsen

Examiner: **Lars Nielsen**

Linköping, May 23, 1995.

Abstract

It is desirable to measure engine performance for several reasons, e.g. when computing the spark advance setting in spark-ignited (SI) engines. There exists two methods, among others, of measuring the performance, such as measuring the pressure and the ionization current. Since the ionization current reflects the pressure, it is interesting to study if it is possible to extract information from the ionization current about the combustion and pressure.

Three different algorithms for extracting information from the ionization current are studied. The first algorithm, ion peak, searches the "second peak" in the ionization signal. The second algorithm computes the centroid. In the third algorithm a model of the ionization signal structure is fitted to the ionization signal.

The algorithms are tested in four operating conditions. The first algorithm uses the local information around the second peak and is sensitive to noise. The second algorithm uses a larger portion of the ionization signal, which is more stable. It provides promising results for engines with a clear post flame phase. The third algorithm, ion structure analysis, fits an ideal model to the ionization signal. The algorithm provides promising results, but the present implementation requires much computational effort.

Key Word: Ionization current, pressure peak, spark timing.

Acknowledgments

Notation

Symbols

θ	Crank angle.
$I(\theta)$	Ionization current.
$Cr(\theta)$	Crank signal.
S_θ	Subset of crank angles.
S_i	Subset of indices.

Abbreviations

(A/F)	Air to fuel ratio.
EGR	Exhaust gas recycling.
DAQ	Data Acquisition.
TDC	Top Dead Center of the crank position.
θ_{pp}	Crank angle at the pressure peak.
λ	Relative air/fuel ratio, $\lambda = 1$ stoichiometric mixture.

Contents

List of Figures

List of Tables

1 Introduction

In spark-ignited (SI) engines today, the ignition timing is computed based on several parameters, e.g. engine speed, and engine load. However, it is not possible to optimize all parameters that affect the ignition timing, therefore trade-off's are made in the static schemes used. A controller for the spark advance based on properties measured during combustion, e.g. pressure or ionization current, could balance these trade-off's and thus improve performance.

The ionization current reflects many parameters in the combustion and among them the pressure, which is an important possible variable in spark control. One advantage with measuring the ionization current, instead of the pressure, is that it makes use of already existing equipment, commercially available in cars. The study of what properties of the ionization signal to use and how to extract them, is an interesting research area.

To give a background to the combustion and ionization current, a literature study is performed and presented. The study regards the peak pressure concept and the ionization current phenomena. Three different algorithms, aiming at spark advance control, using different properties of the ionization signal are implemented and tested. The three algorithms are, ion peak algorithm, ion mass center algorithm, and ion structural analysis. The ion peak algorithm is based upon the knowledge that the ionization signals second peak is correlated with the pressure peak, therfore it searches such a peak. The ion mass center algorithm computes the centroid of the ionization signal. The ion structural analysis fits a model of an ideal ionization signal to the measured, giving parameters to study.

1.1 Organization of the Thesis

This thesis has four main parts where Section 3 is the first part. It is a short summary of the combustion process and the peak pressure concept. Furthermore it consists of a summary of several articles which describe the ionization current phenomena and some applications from it. Section 4, being the next part, contains a description of the measurement equipment used to collect the data. The preprocessing of the data is also described. The next part of the thesis consists of the two Sections 5 and 6, where Section 5 contains the main ideas for the algorithms tested in this thesis. Section 6 describes the algorithms more comprehensive and some details in the algorithms are sorted out.

In Section 7 the results of the algorithms are discussed. A comparison between the algorithms and their results is also described in this section, as well as some possible extensions to the work. This section is the fourth and last main part of this thesis. A discussion of the work and the conclutions are contained in Section 8. A pre study performed on data from Mecel AB is described in Appendix A. It is used as a basis for some of the work done in this thesis and is therefore presented.

2   Background

In Spark Ignited internal combustion engines (SI engines), the work produced depends on the ignition timing, as well as several other parameters. Late ignition timing does not make use of the the full stroke of the piston, and less work is produced. Early ignition timing produces a high pressure too early, i.e. when the piston is moving up, and work is lost.

It is a well-known fact that the pressure time history shows the efficiency of the combustion, i.e. from the pressure it is possible to compute the work produced during one cycle [8]. Information from the pressure is thus one possibility to compute a better point of ignition, and retrieve a more efficient combustion by controlling the ignition timing [14].

Implementation of a pressure based controller is connected with several problems, e.g. high cost, unstable sensor performance, changes in combustion due to the sensor, and no place for installation of a sensor [16]. However, there exists an alternative for measuring the pressure, this is to measure the ionization current inside the cylinder.

The ionization current reflects many parameters in the combustion and among them the pressure. The greatest advantage when measuring the ionization current is that it use existing and commersially available equipment, such as the spark plug and electronics. The ionization currents are in some systems already measured, the only thing that has to be added is computation of the ignition timing.

3 Combustion

The combustion process and some properties associated with it are described in this section. The important properties are the pressure development and the ionization currents. A comprehensive description of the combustion in internal combustion engines is given in Heywood [8]. Regarding the ionization currents two principles of measuring are described. The ionization process description is a summary of some articles about this subject.

3.1   The combustion process

During the compression in the cylinder, a spark ignites the gas mixture and the combustion begins. The combustion increases the pressure and temperature in the cylinder. The pressure in the cylinder during the compression and expansion phase is shown in Figure 3.1. The dashed curve shows the pressure in the cylinder when no combustion
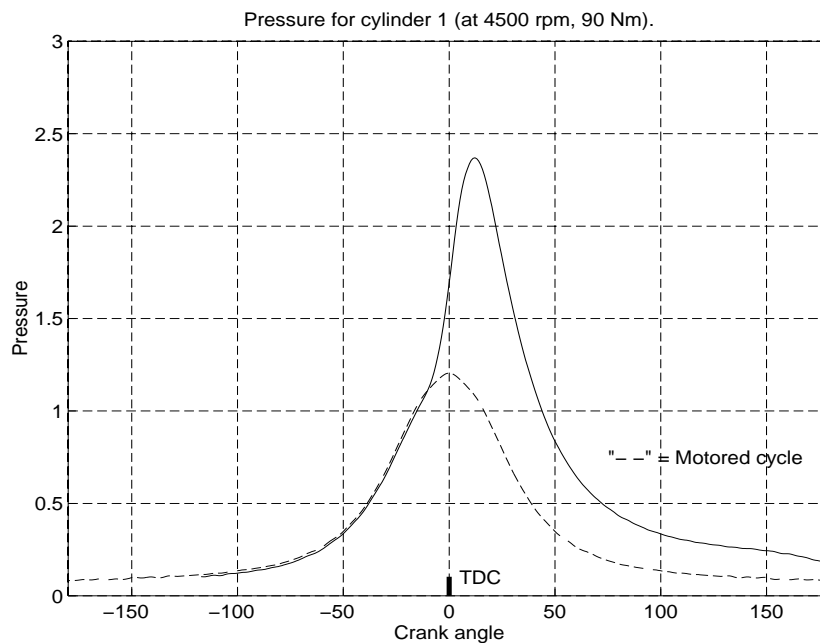
Figure 3.1. Pressure development for a motored cycle and a cycle where combustion occurs.

occurs, called the motored cycle. The term background pressure is in some articles used for the pressure during the motored cycle. At approximately 15° before TDC (TDC is an abbreviation for Top Dead Center) the pressure begins to increase over the background pressure, as shown in the figure. After the crank has passed TDC the volume starts to increase, still the pressure increases due to the combustion. At approximately 15° after TDC the pressure reaches its maximum. At this point the combustion is almost completed and the volume expands more rapidly, hence the pressure begins to decrease.

When the pressure increases over the pressure for the motored cycle, additional work is transferred to or from the engine. In Figure 3.1 the pressure starts to increase over the background pressure at 15° before TDC. In order to get the piston to TDC, position (b) in Figure 3.2, additional work has to be transferred from the engine. When the piston
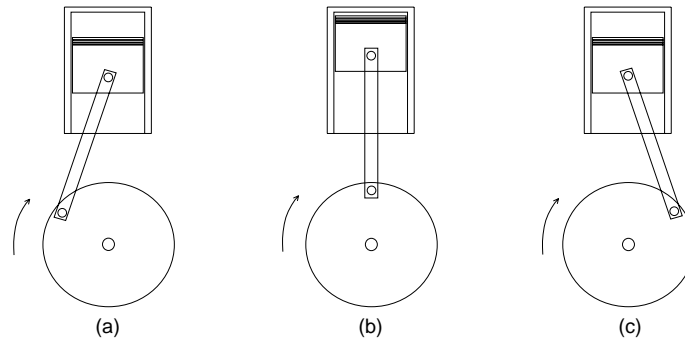
Figure 3.2. The crank at three different angles: (a) before TDC, (b) at TDC, (c) after TDC.

has reached past TDC, the additional pressure transfers work to the engine. Since work is transferred to the engine after TDC it is desirable to have as high pressure as possible after TDC. The data plots in Figure 3.3 visualize these statements. Another
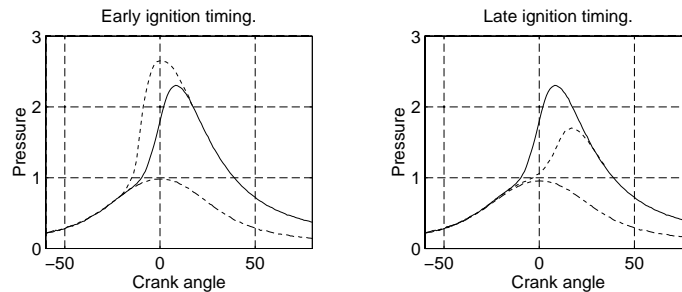
Figure 3.3. Pressure development for cycles with early and late ignition timing (dashed). The motored cycle (dash-dotted) and the optimal pressure cycle (filled) are also shown.

interesting fact is that the lever at TDC is zero, and it increases with the crank angle until approximately 90° after TDC. In order to produce as much work as possible it is desirable to keep the pressure high as long as possible during the expansion phase. When the crank angle increases, the volume also increases and hence the pressure decreases. Lower pressure gives less force on the piston which results in less produced work to the engine. As a result, the pressure time history plays an important role for the work produced during each cycle. The pressure time history must hence be positioned in some manner to produce optimal work.

In order to position the pressure time history to produce maximum work, the spark advance must be varied with different working conditions for the engine. The spark advance for an engine depends on many different parameters, e.g. engine speed, engine load, (A/F) ((A/F) is an abbreviation for Air/Fuel ratio), fuel composition, air temperature, air humidity, and several other factors. The engines of today measure several of these parameters and then computes a spark advance based on these measurements. The computation is based on knowledge about the engine together with extensive testing and measuring during the design of the engine. However, it is not reasonable to measure all parameters since it would be very expensive. It is also expensive to perform the testing associated with the design of such a system. A control algorithm could be designed to position the cylinder pressure time history in an optimal manner e.g. to maximize the work, or to minimize the emissions. The angle to peak pressure, θ_{pp} dashed line in

Figure 3.4, can be used for optimum spark timing [14]. This result has been reported for parameters that affects the flame speed, and for changes in humidity. Humidity is important since it is the single largest environmental disturbance to optimal spark timing.
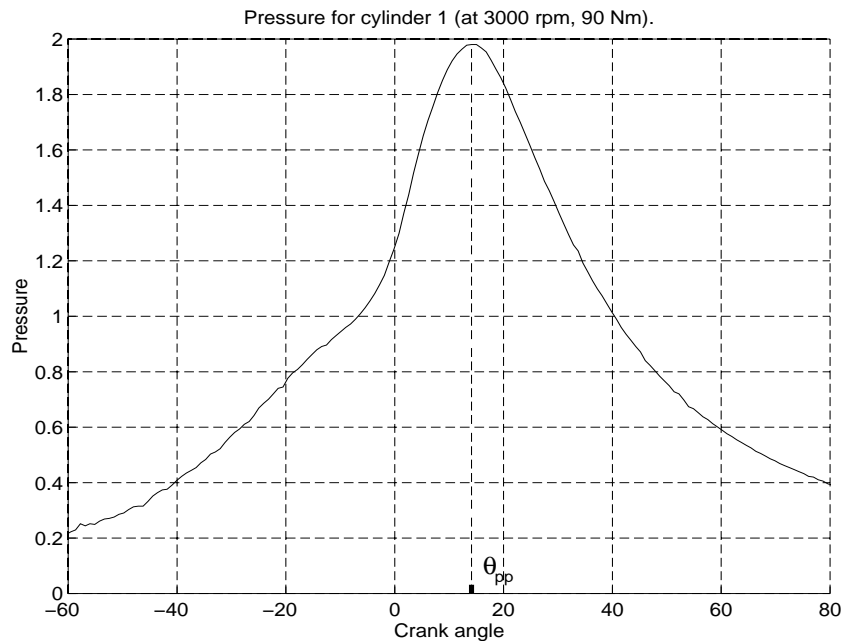
Figure 3.4. The pressure signal shown from 60° before TDC to 80° after TDC. The angle to peak pressure (θ_{pp}) is approximately 15° after TDC.

The angle θ_{pp}, for optimum work, varies between ten and twenty degrees after TDC [14]. A non-comprehensive explanation to the peak pressure concept is: If the pressure has a maximum at TDC a lot of work is needed to position the piston there and the engine would hence lose power. At TDC the torque is also zero. When the angle after TDC increases, the lever increases and gives greater torque, but the volume also increases which gives less pressure. Hence there is less power produced to the engine. From this it can be understood that there is an optimal point for the pressure peak.

3.2   The ion generating process

The ionization process can shortly be described as follows; The heat in the flame front ionizes the gas in the combustion chamber and the gas becomes conductive. An electric field is applied in the combustion chamber and the generated current is measured. The ionization degree depends on the temperature in the cylinder which is strongly connected to the pressure of the cylinder. The result is that the ionization current contains information about the combustion process and the pressure.

The chemical reactions in the combustion process are very complex, in a simplified way C_xH_y molecules reacts with oxygen molecules and generate CO_2 and water. Reaction (3.1) is an example of a reaction considered usual in an internal combustion engine [8], [16].

$$C_3H_8 + 5O_2 \longrightarrow 3CO_2 + 4H_2O \tag{3.1}$$

However, these are just the ideal results from the combustion, the actual combustion has several stages where molecules get ionized by the heat and then recombine to other more stable molecules. Some elementary reactions that create ions [16] are

$$CH + O \longrightarrow CHO^+ + e^-$$
$$CHO^+ + H_2O \longrightarrow H_3O^+ + CO$$
$$CH + C_2H_2 \longrightarrow C_3H_3^+ + e^-$$
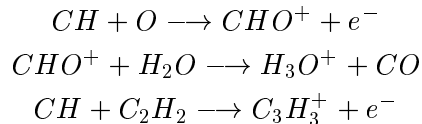
There are other ions than the above that are generated during elementary reaction, for example CH_3O^+, OH^-, and O^{2-}. A considerable amount of both H_3O^+ and $C_3H_3^+$ are also generated, and as their residual time is relatively long, these positive ions and electrons become carriers of ionic currents [16]. In, "Electrical aspects of combustion" [12], the ions generated in the combustion are described, as well as the processes and constraints that generates and recombines ions.

There are four different processes that result in ionization, namely: ionization by collision, electron transfer, ionization by transfer of excitation energy, chemi-ionization. There are three different types of recombination, these are: three body recombination, dissociative recombination, mutual neutralization.

To obtain a property that reflects the ionization degree, a probe is inserted into the combustion chamber. This probe is biased in order to create an electric field that attracts and rejects ions in the vicinity of the probe. It is a well-known and confirmed fact that a positively biased probe gives higher signal levels in order of magnitude [5], [6]. One proposed explanation for this phenomena is that in the combustion chamber the ions are dominated by the electrons. Since they are much smaller and has a relatively larger area to get attracted to they have the possibility to create larger current. Equilibrium calculations for the temperatures present in the combustion chamber also supports this theory. In the exhaust manifold the temperature is lower, and here some heavier ions are dominant over the electrons. The difference between a positively- and a negatively-biased probe is not as big as in the combustion chamber [5].

3.3   Measurement principles

The spark plug or a separate pin inserted into the combustion chamber, is used as a probe for detecting the ionization levels. Examples of these are shown in Figure 3.5. Other sensors, similar to these shown in the figure, also exists [2]. The signals studied in this thesis were measured using the spark plug. The spark plug has the advantage that it is already mounted, i.e. no extra cost for installation of an additional probe. A potential disadvantage is the ignition pulse since no useful ionization signal is retrieved during this phase. When the ignition has ended, the spark plug is available for measurement during the remaining part of the combustion. The combustion process is started by the spark plug and it has hence a good monitoring position over the process.

The principle for measuring is, as described earlier, to create an electric field in the combustion chamber and measure the current through the spark plug gap. The circuit that generates and measures this current consists of; voltage source, spark plug, spark gap, down to the engine ground.

One way to measure is to apply the test voltage directly to the spark plug, as in Figure 3.6. The measuring equipment is positioned at the high voltage side of the ignition coil, which implies that the circuits must be protected from the high voltage pulses that generates the spark. To protect the measuring circuits a high voltage diode

(a) (b)
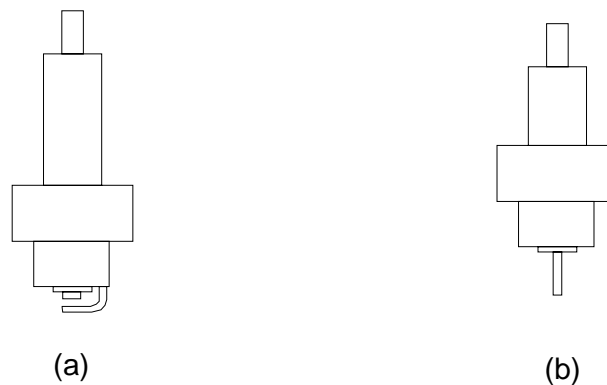
Figure 3.5. Two different probes. (a) The ordinary spark plug. (b) A separate probe similar to the spark plug.
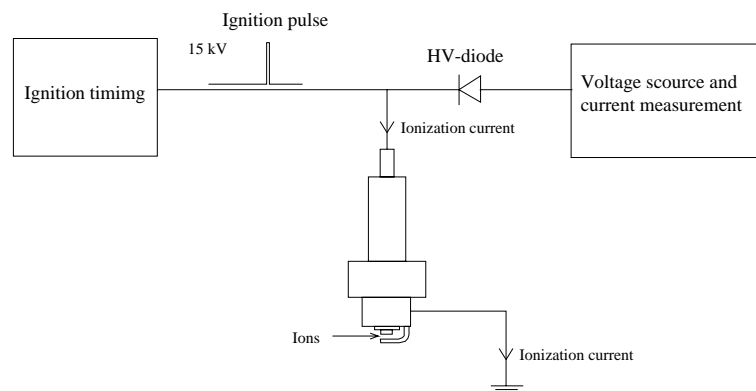
Figure 3.6. Ionization measurement at the high voltage side of the ignition coil.

(HV-diode) is connected as shown in the figure. These diodes do not instantly open after the high voltage pulse, that creates the spark, has ended. The reason is that the diodes have a capacitance which must be discharged, after it is charged by the ignition pulse. Hence, some interesting part of the ionization current might be missed [10].

Another way to measure the ionization currents is to apply the test voltage at the low voltage end of the coil, and measure the current through the coil. This was proposed by Mecel AB [7]. This measuring technique does not require HV diodes to protect the circuits. Since the coil does not affect the test current that much, and there is no high voltage pulse, it is a good place for measuring the ionization current. A schematic figure showing the principle for this measurement circuit is shown in Figure 3.7. This measurement method is used to collect the data studied in this thesis.

Both principles of measuring use a positively biased probe for the same reasons as discussed earlier in Section 3.2.

3.4 Characterization of the ionization current

The properties of the ionization current signal will now be discussed. In Figure 3.8 one characteristic ionization signal is displayed. It has three phases; Ignition, Flame front and Post flame. In the ignition phase the signal is disturbed by the ignition pulse generated by the coil. In this phase it is not possible to say anything about the ionization
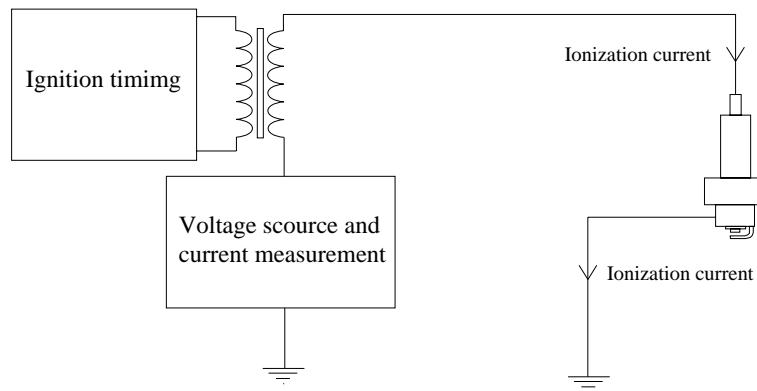
Figure 3.7. Ionization measurement at the low voltage side of the ignition coil.
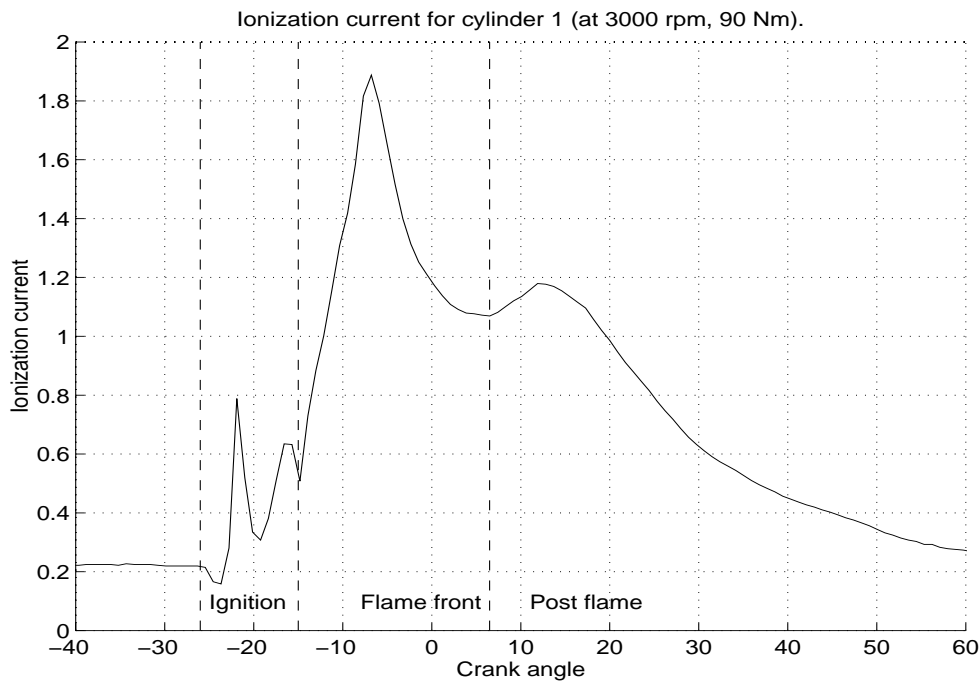
Figure 3.8. Ionization current showing the three phases; Ignition, Flame front, Post flame.

current.

The next phase is the flame front. Here the high signal level is due to the high ionization degree at the flame. In the flame many different ions are generated, some recombine quickly to more stable molecules while other have longer residual time. The flame is only close to the probe some short period, when it propagates through the combustion chamber. This explains why the flame front is a high peak which quickly decreases. When this phase is over only the more stable ions remain.

The post flame ionization is mostly constituted of H_3O^+, CO^- and their hydrates. At higher temperatures, equilibrium considerations suggests that electrons are also present [6]. The post flame region is a superposition of an ionization level decay from the flame front, and an ionization concentration associated with the cylinder pressure. The cylinder temperature and pressure are closely related, ideally $pV = nRT$, and it is thought that the ionization current follows the temperature due to its effects on the

electron concentration. Since the temperature and the pressure are closely related, the ionization signal follows the pressure to some degree in this latter phase.

As mentioned earlier, the ionization current phenomena is complex and many engine parameters affect the ionization currents. The following parameters affect the ionization current [1], [2], [5], [6].

- Temperature

  The ionization degree depends on the temperature, and therefore the ionization current depend on the temperature. This is easy to understand since increasing temperature means more energy to ionize the molecules, and the result is increasing ionization current. The temperature also affects the recombination rate for the ions. The rate is inversively proportional to the 1.5th power of the momentary temperature [10]. Hence, it does also affect the ionization current.

- (A/F) ratio

  The ionization signal has a maximum for $\lambda = 1$, where λ is the relative air/fuel ratio, corresponding to stoichiometric proportions for the mixture. With lean mixtures (increasing λ) the signal level continuously drops. This phenomena might be due to lower temperature in the combustion process and hence give a smaller signal. As long as combustion occurs there is a measurable signal. At rich mixtures the signal slightly decreases until there is a cut-off, in the signal level, around $\lambda = \frac{1}{1.6}$. This correlates well with the point where soothing occurs. One explanation for this is that the charged species become attached to the sooth particles and get more immobile [6]. The air to fuel ratio, λ, also affects the flame front phase. In fact it has been shown to correlate well with the initial slope of the flame front phase [13].

- Time since combustion

  The recombination of charged species is rapid, and therefore the concentration of ions drops quickly after the flame front. When the concentration gets low the recombination rate decreases, and thus useful signals can be obtained even in the exhaust system [6].

- EGR

  Since EGR, Exhaust Gas Recycling, affects the temperature, it also affects the level of ionization current [10]. EGR also makes the signal vary in time, due to "clouds" of EGR-gas which pass the ionization sensor. Since the ionization level is lower in the EGR-gases the effect is that the signal drops when the "cloud" passes.

- Fuel composition

  Different fuels give different signals probably dependent on the different composition of hydrocarbons in different fuels. It is a well-known fact that the fuel has very large fluctuations in composition. Lead additives in the fuel does also affect the ionization degree, by increasing the ionization level due to their slow recombination rates [2].

- Leakage currents

  The resistance value of the spark plug can change from cycle to cycle, and give large fluctuations in signal levels. Measurement of the plug resistance at stationary

engine is of limited use [6]. The changes in spark plug resistance are due to several effects. One is that a sooth particle might get attached to the gap in the spark plug and change the electrical aspects of it.

- Engine load

  The signal level gets larger with higher engine loads [5]. This is due to higher temperatures in the combustion, and more reactants in the combustion chamber.

- Humidity in the air and many, many more.

  Humidity is the single largest environmental disturbance to the pressure development in the combustion, hence it also affects the ionization signal.

As it can be seen, there are many parameters affecting the ionization currents. This imposes that one must be cautious, drawing conclusions about parameters from the ionization currents. On the other hand, when there are several parameters affecting the ionization currents, these interactions can be used backwards to derive the interesting parameters. This points out that it might be possible to use the ionization current for deriving important combustion parameters.

4 The measurement situation

A description of the engine and the data acquisition equipment, used to collect the test data, is contained in this section. The first part describes the engine and some of its interesting parameters. Three signals, pressure, ionization current and crank signal, are sampled and studied.

A pre study was performed on data from other engines, as discussed in appendix A. The datasets in the pre study were collected by Mecel, and the organization of these tests and measurements is not mentioned in this thesis.

4.1 Engine description

The engine is the one used in the laboratory of the division of Vehicular Systems at Linköping University. It is a SAAB 2.3 liter, four cylinder, 16 valve, four-stroke engine with fuel injection. The ignition system is modified to provide a measurable ionization signal.

An extra hole is drilled into the cylinder, where a pressure sensor is inserted. The sensor is a quartz pressure transducer [3], which is positioned near the spark plug. Figure 4.1 shows a schematic picture of the situation. The temperature in the combustion
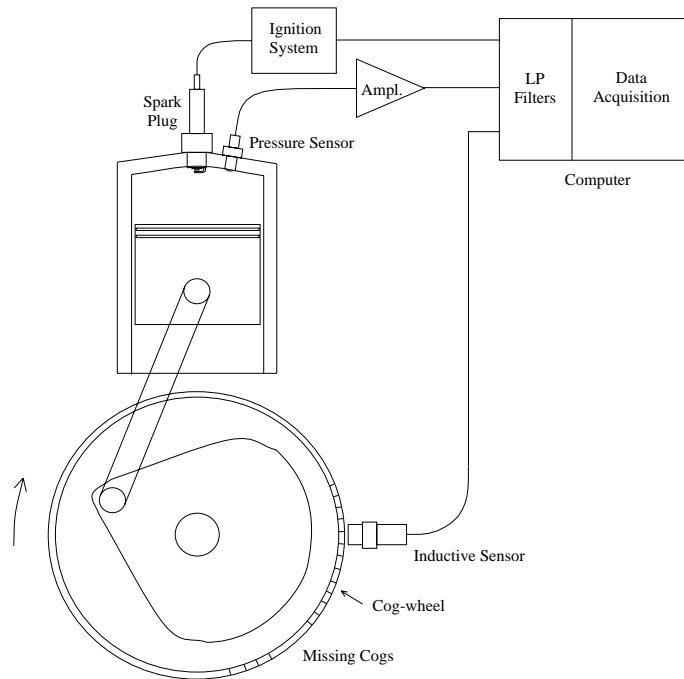
Figure 4.1. Schematic figure of the engine and the sensors used.

chamber affects the pressure sensor, and changes the characteristics for it. Very high temperatures during long periods might even cause damage to the sensor. In order to reduce this influence and to reduce the temperature stress, the pressure sensor is cooled by an external cooler. The piezo-electric sensor gives a low signal level that is amplified by a special amplifier [4]. After the amplifier the signal has a level appropriate for the data acquisition equipment.

The ionization current is the second signal that is measured. The Mecel principle for measuring is used. The principle is described in Section 3.3. One detail of the

measurement which was left out earlier, is the signal level. The current measurement circuit gives a signal level between zero and twelve Volts. The signal value is proportional to the current in the circuit, therefore it does not give the actual value of the ionization current.

The third signal is the crank signal, which is important for retrieving correct engine data. In Figure 4.1 the sensor, fly-wheel, piston, and bore are displayed. To the fly-wheel a cog-wheel is attached. This cog-wheel has two missing cogs that are used to detect a reference position. The missing cogs are placed at $117.5°$ before TDC. Close to the cog-wheel an inductive sensor is placed. From this signal the crank angle at each sample can be computed, these computations are described more closely in Section 4.3. This signal is further on referred to as the crank signal.

The three measured signals are shown in Figure 4.2. They are plotted for one cycle which is equal to two turns in a four-stroke engine. In the measurement equipment the ionization signals from two cylinders are added together. This explains the appearance of the ionization current in Figure 4.2. The missing cogs shows clearly at approximately $240°$ in the crank signal.
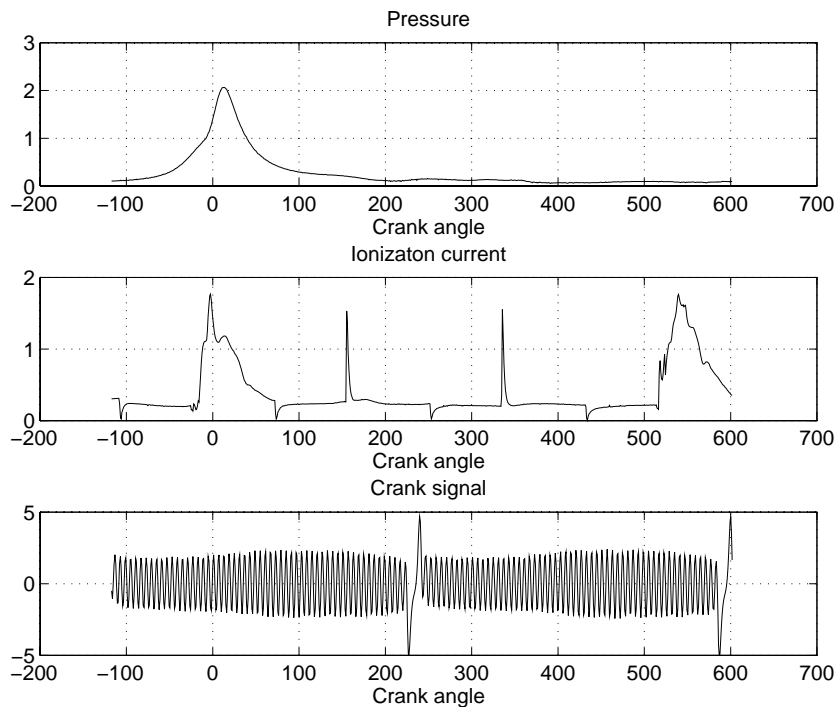
Figure 4.2. The three measured signals; Pressure, Ionization signal and Crank signal.

4.2   Data acquisition

A PC-based DAQ-card is used to sample the signals from the engine [17]. DAQ is an abbreviation for Data AcQuisition, and this abbreviation will be used further on in the text both for Data Acquisition and the DAQ-card. Before the signals are sampled they are voltage-divided by a factor three and LP-filtered in order to avoid aliasing. The filter is an analog passive voltage divider, and has a cut off frequency at approximately $15kHz$. The sampling rates are set such that $1°$ corresponds to one sample, for a engine

speed of $4500rpm$ this is approximately $27kHz$. The DAQ does not sample the channels simultaneously. The delay between two channels is $\sim 1\mu s$, which corresponds to a difference in crank angle of $0.036°$ at $6000rpm$. This is not much since the sampling rates correspond to $1°$ and the engine mostly runs at less than $6000rpm$. From the DAQ-card, and an application program for it, the data is written as a text file in regular ASCII-format. This file is then loaded into Matlab or any other data processing program for further processing of the data.

4.3 Preprocessing of data

In order to study the engine data it must be related to the crank position, therefore the crank angle at each sample is computed. Then the data can then be related to the engine state.

The crank signal contains angle information for the samples. This information has to be computed from the sampled crank signal. In Figure 4.3 the crank signal is plotted against the samples. The upper plot show the signal during one cycle, and the lower plot is an enlargement of the signal directly after the missing cogs.
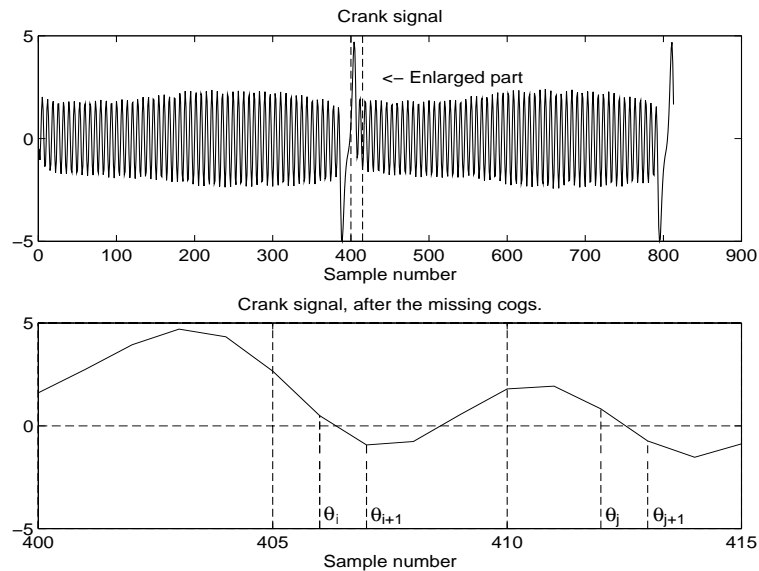
Figure 4.3. Crank signal with the missing cogs marked.

The important points in the signal are marked in the lower plot of Figure 4.3. These are θ_i, θ_{i+1}, θ_j and θ_{j+1}. The zero crossing between θ_i and θ_{i+1}, in the figure, corresponds to a crank angle of $117.5°$ before TDC. The following zero crossings from positive to negative appear with a distance of $6°$. Based on these zero crossings and the missing cogs, the crank angle at every sample can be computed in the following way. Let Δ_i denote the distance to the zero crossing from θ_i, and similar for Δ_j. Using a linear model of the crank signal, between sample i and $i+1$, the following expression gives Δ_i,

$$\Delta_i = \frac{Cr(\theta_i)}{Cr(\theta_i) - Cr(\theta_{i+1})}$$

With these conventions $6°$ corresponds to the distance,

$$6° \propto j + \Delta_j - (i + \Delta_i)$$

in samples. Let the difference in crank angle between two samples be denoted D, the above give the following expression,

$$D = \frac{6}{j - i + \Delta_j - \Delta_i} \tag{4.1}$$

The formula for computing the crank angle, θ, at every sample, n, between two zero crossings, m and $m + 1$, is now,

$$\theta_n = -117.5 + m * 6 + (1 - \Delta_i) * D + (n - j) * D \tag{4.2}$$

where n denotes the index for the samples $i+1$ to j, and m the number of the zero crossing relatively the missing cogs. The zero crossing after sample i in the figure corresponds to $m = 0$ and j to $m = 1$.

Equation (4.2) is an equation for computing the crank angle at every sample. The equation is valid between all zero crossings except for the ones around the missing cogs, where D instead is,

$$D = \frac{18}{j - i + \Delta_j - \Delta_i} \tag{4.3}$$

To summarize, first every zero crossing in the crank signal is searched, then the positions for the missing cogs are detected. After this the crank angles to every sample is computed from equation (4.2) using the appropriate D from (4.1) or (4.3).

4.4   Engine operating points

Four datasets were collected at different operating points for the engine. The engine speed and load at these operating points are shown in Table 4.1. During the tests it was not possible to affect other engine parameters than engine-load and speed. The engine control system handles all other parameters itself.

Engine speed (rpm)	Engine load (Nm)
3000	50
3000	90
4500	50
4500	90

Table 4.1. Operating points for the tests.

In Figures 4.4 to 4.7 five cycles from each operating point are displayed.   There are some similarities between the operating points. First the pressure for two operating points with the same load have almost the same level in pressure. It is the pressure development up to the peak that is different, which is due to the difference in sampling rate at these operating points. When the engine is run at different engine speeds, there
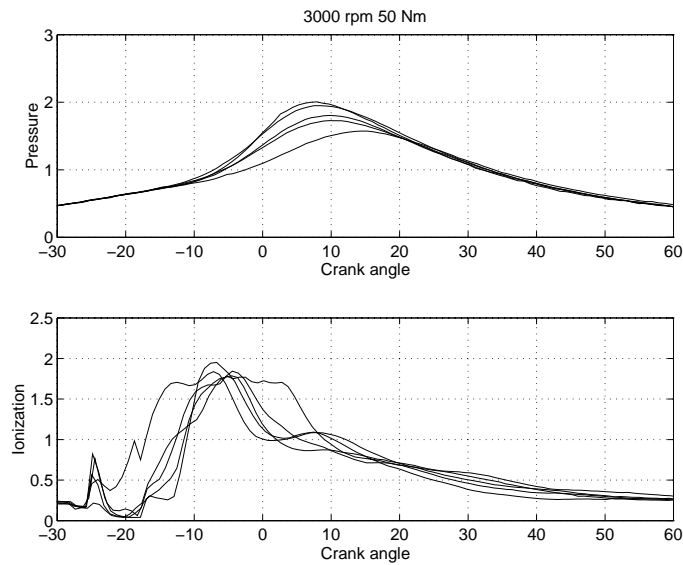
Figure 4.4. Five consecutive cycles for the operating point 3000 *rpm*, 50 *Nm*.
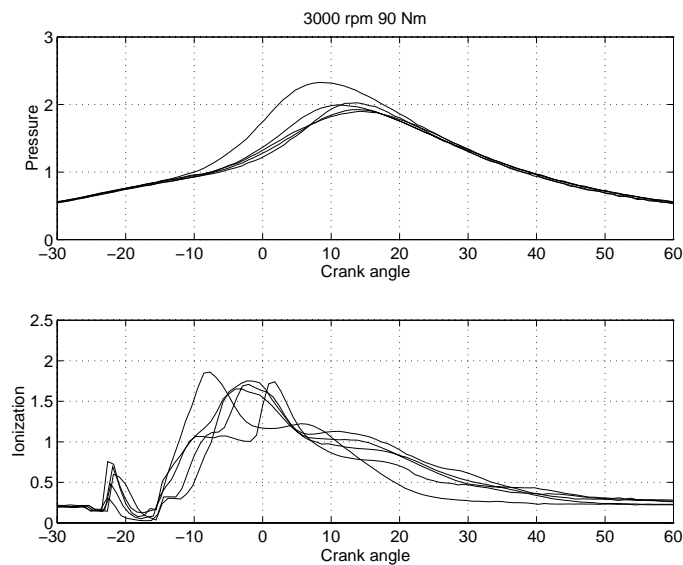
Figure 4.5. Five consecutive cycles for the operating point 3000 *rpm*, 90 *Nm*.

is a difference in the crank angle corresponding to the flame propagation time. Hence, the pressure development is somewhat dissimilar between these operating points.

The ionization also contains some similarities. In this case it is the behavior of the post flame phase and not the signal level which is similar. This is best visualized by studying the Figures 4.4 and 4.5. The post flame phase for the operating point with load 90 *Nm* is more visible than for the one with load 50 *Nm*. For the operating points with engine speed 4500 *rpm*, Figures 4.6 and 4.7, the signal level is larger, but the same phenomena exist for this engine speed.

The plots 4.4 to 4.7 shows that there are large cycle to cycle variations in the pressure and especially in the ionization signal. Another reflection is that it is difficult to separate the post flame phase from the flame front phase.
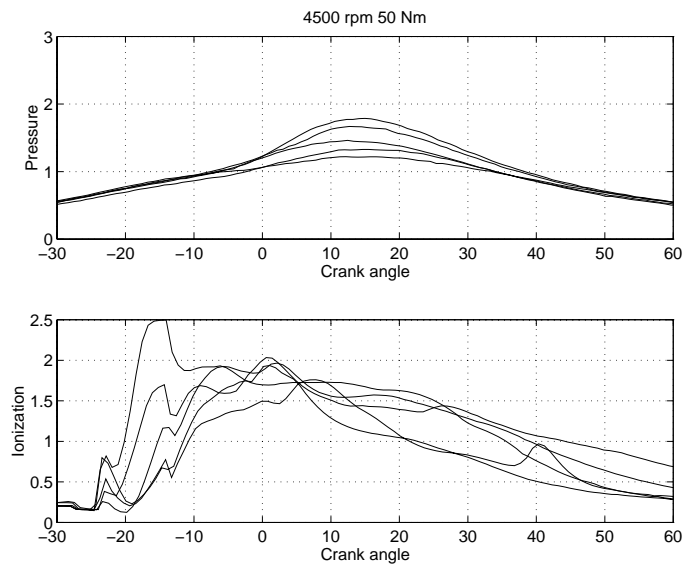
Figure 4.6. Five consecutive cycles for the operating point 4500 rpm, 50 Nm.
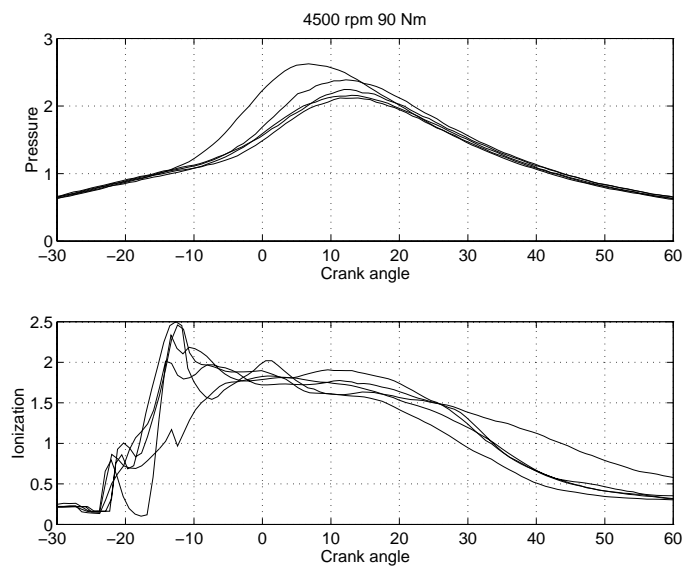
Figure 4.7. Five consecutive cycles for the operating point 4500 rpm, 90 Nm.

5   Main ideas for the algorithm

As mentioned in Section 3.2 the pressure and the ionization are connected to each other. From this knowledge three algorithms are derived. These use three different aspects of the ionization signal. The first algorithm searches the local maximum in the post flame phase. The second computes the centroid of the ionization signal, it is called the mass center algorithm later on. The third algorithm fits a model of the ideal ionization signal to the measured signal.

The main ideas for the algorithms are described in the Sections 5.2 to 5.4. The implementation of the algorithms is presented in Section 6.

5.1   Pressure versus ionization current

The ionization signal in Figure 3.8 shows the three phases; Ignition, Flame front, and Post flame. It was mentioned that the post flame phase is a superposition of the pressure and the ionization decay. Since this part consists of ionization from the pressure it is interesting to study and to compare it with the pressure. The question is therefore, how to find the post flame phase and what information to use from the specific phase.

In Figure 5.1 both the ionization current and the pressure signal are displayed. This
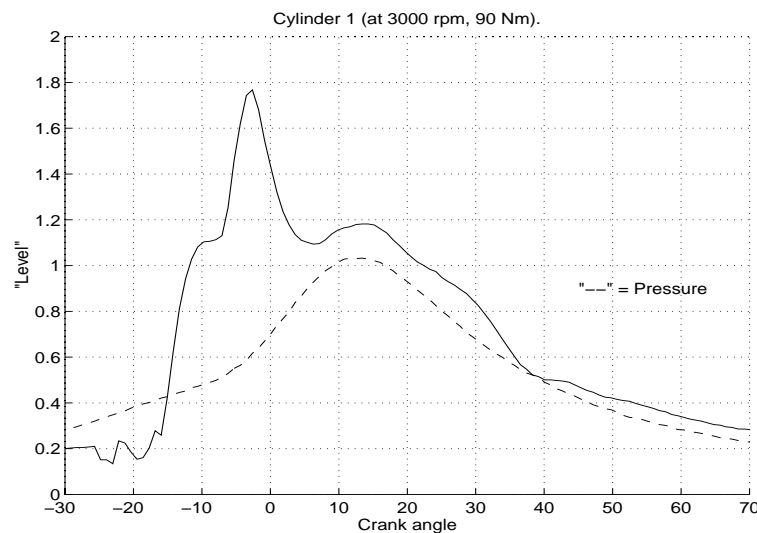
Figure 5.1. Plot of pressure and ionization current in the same diagram.

figure supports the idea that there is a correlation between the pressure and the post flame phase. In this case the ionization signal is "well behaved" since it consists of two distinct peaks. However, in most cases there does not exist two distinct peaks. One example of this is shown in Figure 5.2. The signal reflects the pressure, and it is interesting to study if it is possible to use any information from this part.

This is a short description of the connection between the pressure and ionization signal. All three algorithms are mainly ideas of how to extract useful information from the post flame phase.
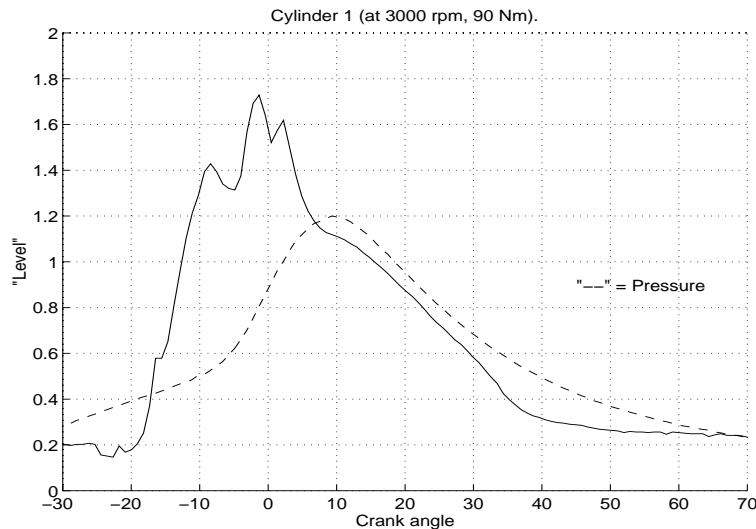
Figure 5.2. Plot of ionization and pressure showing when no peak in the ionization signal occurs.

5.2 Algorithm 1: Ion peak algorithm

The first idea is to use the local maxima in the post flame phase as approximation for the pressure peak. This idea is patented by Bosch [11], and the algorithm is constructed from the guidelines within their patent. In Figure 5.1 the position for the post flame peak correlates well with the pressure peak. This fact is the corner stone for the first algorithm. It searches the local maximum using the first and second order derivative. When computing the derivative of a signal, the high frequency noise is amplified. In this case it is interesting to study the slow fluctuations of the signal, accordingly it is appropriate to filter the signal. A smoothing filter eliminates the high frequent noise and smoothes the signal. The filter used, a non-causal smoothing filter, is described in Appendix B.

The first peak varies in magnitude and position, therefore the flame front is the largest problem for this algorithm. The algorithm must get past the flame front and not get stuck at a point in this phase. The first idea to overcome this problem is to take the second peak found in the signal. However, it is not certain that the signal has just one peak in the flame front. An example of when the flame front consists of two peaks is shown in Figure 5.3, Observing that the last peak in the flame front lasts past TDC, in both the plots 5.3 and 5.4, this rise a demand for a late search start.

The pressure peak might appear directly after TDC, which give the demand for a search start directly after TDC. Therefore, when selecting a search start a trade-off must be made. The search start is selected to 5° after TDC. The reason is that the earliest position for the pressure peak in the pre-study is later than 5° after TDC. This is also the case for the data collected in the main study. In other engines the ionization signal has different characteristics, which leads to that the search start should be chosen differently. There is still an uncertainty whether or not the algorithm will find the right peak. It can get stuck at peaks in a late flame front phase.

After the search start is found, the search for a maximum in the ionization signal begins. A local maximum is characterized by a zero crossing in the derivative from positive to negative. Hence, such a zero crossing is searched for. If there exists a local
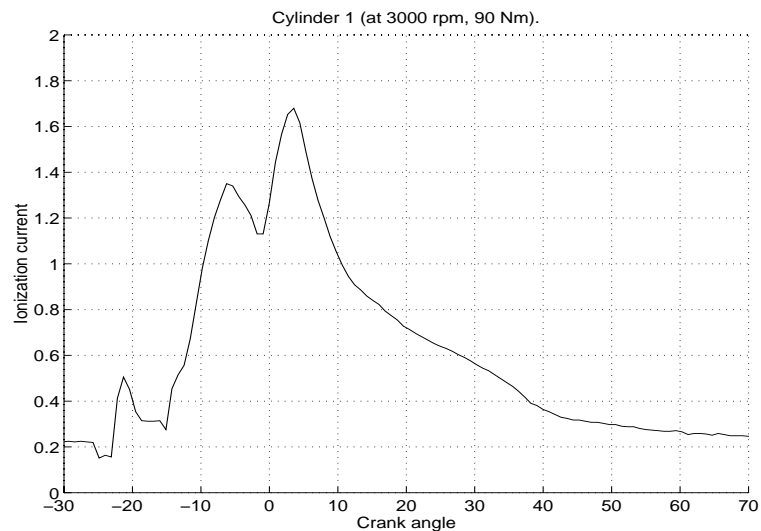
Figure 5.3. Plot of the ionization signal showing two peaks.

maximum in the post flame phase after the start point, it will be found. Though, there does not always exist a peak in the post flame phase, this case is shown in the Figures 5.2, 5.3, and 5.4. If a maximum does not exist in the post flame phase the point returned does
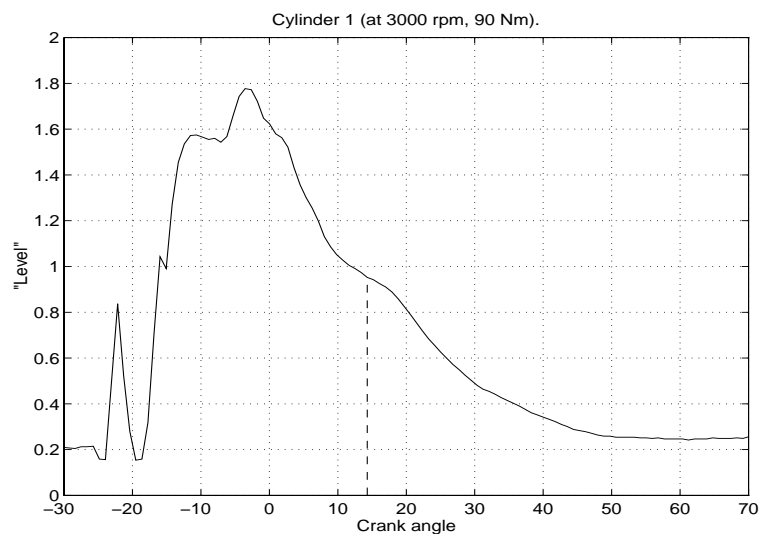
Figure 5.4. Plot of the ionization current showing when the first peak is late and distorts the post flame phase.

not correlate with the pressure peak. In Figure 5.4 the point retrieved by the algorithm is positioned outside the plotted range. When the algorithm returns a value greater than a certain value, the post flame does not contain a local maximum. Consequently, this can be used as a criterion to search another point.

When the first order derivative does not return a suitable value the second order derivative is used. More closely the inflexion point with a sign shift from positive to negative is used. An inflexion point is where the second order derivative has a zero crossing. This point corresponds to where the derivative is "largest" and begins to

decrease. Visually this is where the signal is leaning least downwards. In Figure 5.4 this
point is marked with a dashed line. It is possible that no inflexion point exists in the
interval. In that case, it is questionable what the algorithm shall return. One idea is to
take the point found in the previous cycle. Another is to use the mean values of some
of the latest points found.

   When this algorithm was derived, it was for the sake of testing the basic principle
that the post flame peak correlates well with the peak pressure. The algorithm might
therfore not be the best algorithm, but it serves the purpose of testing the basic principles
and comparing it with other algorithms.

5.3   Algorithm 2: Ion mass center

The second algorithm computes the centroid, or center of mass, of the ionization signal.
The algorithm will be referred to as mass center algorithm from now on. It is not just one
algorithm that is implemented and tested but several variations of the same idea. The
basic idea is that the ionization signals varies from cycle to cycle, and hence give varying
shapes of the signal. The ion peak algorithm only takes the local appearance around
the post flame phase into account, which make the point vary a great deal from cycle to
cycle. The mass center, takes all values from the cycle into account, and cycle-to-cycle
fluctuations of the appearance might not affect the mass center that much.

   The first thing to study is whether or not the mass center for the whole ionization
signal is correlated with the pressure peak. The next is if different ways of computing
the mass center give better result than the ordinary mass center method. The ordinary
mass center is computed by the equation,

$$\frac{\int_{cycle} \theta I(\theta) d\theta}{\int_{cycle} I(\theta) d\theta}$$

If the ionization signal is raised to some power, p, and the mass center is computed for
this new function, another point retrieved. Mathematically this is,

$$\frac{\int_{cycle} \theta (I(\theta))^p d\theta}{\int_{cycle} (I(\theta))^p d\theta}$$

This mass center takes more account to the larger values of the signal, which make mass
center moves towards the maximum. It is interesting to study how much this mass center
behaves and correlates with the pressure peak for different different powers, p.

   A large flame front might disturb the interesting properties of the mass center. Com-
pare the signals in Appendix A with the ones in Figures 5.1 to 5.4. These signals demon-
strates a considerable difference in the flame front. This indicates that it is interesting
to dispose the flame front and correct the signal, and then study the mass center for this
new signal.

   To correct the signal, a point at the end of the flame front or the beginning of the
post flame must be found. In the pre study, Appendix A, the inflexion point shows
some nice properties, which reflects the behavior of the ionization signal. Therefore the
inflexion point is used as a point for discarding the earlier values. This point will be
called DP (Discarding Point), and it is selected as the point where the derivative of the
signals, has its maximum after the flame front. This is the same as when the second
derivative is zero and has a shift in sign from positive to negative, Figure 5.5 visualizes
this for a smoothed ionization signal.
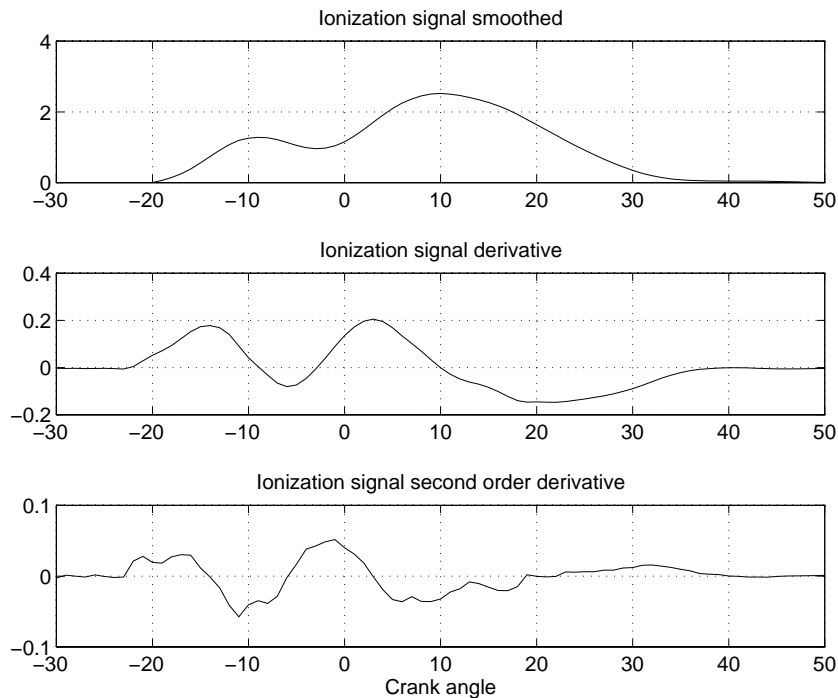
Figure 5.5. The ionization signal with the first and second order derivatives.

When the signal is cut at DP it is desirable to extrapolate the signal shape, before DP, in some way before the mass center is computed.

Correction of the signal

Three different ways of correcting the ionization signal by extrapolation are considered. The first correction is to set the signal equal to zero before DP, and equal to the ordinary ionization signal after DP. The second correction is to take a straight line and continue in the direction of the signal derivative at DP. At samples before the point where the line reach zero, set the signal equal to zero. The third is to correct the signal with an second order polynomial. The correction shall have the same slope as the ionization signal at DP, it must also have the minimum equal to zero. In Figure 5.6 the three different corrections are displayed.

There are several other ways of correcting the signal which might be better than these three, but these corrections are simple and do not require much computational effort.

Some problems with the second and third corrections exist if the derivative at DP is small or negative. This will in these cases generate a non physical correction. The condition in such a case is that the derivative is to small. Hence, it is possible to check the derivative, and if it is less than a certain value it is replaced by a default value. Figure 5.7 displays a plot where the derivative is limited and replaced.

When the signal has been corrected, the mass center for the corrected signal is computed using different exponents, p. The different corrections and different exponents leads to different mass centers.
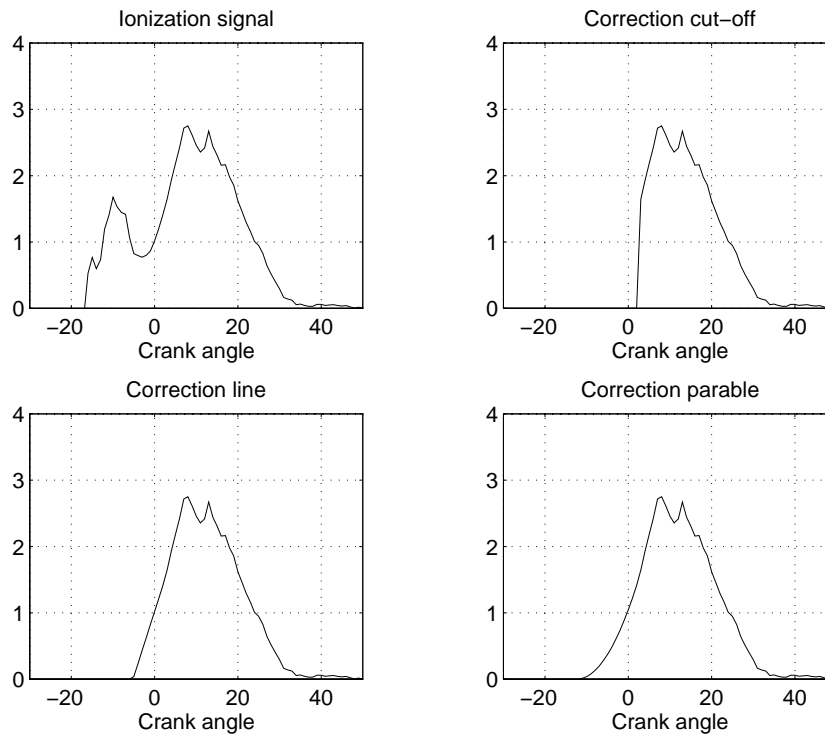
Figure 5.6. The three different corrections for the ionization signal.
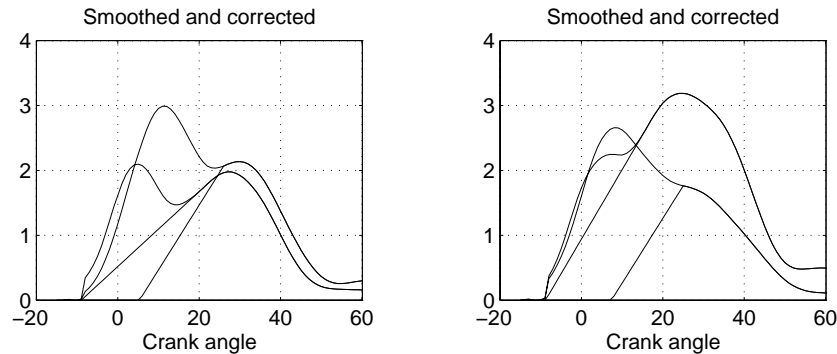
Figure 5.7. Limited corrections for the correction with a line.

5.4 Algorithm 3: Ion structural analysis

The knowledge that the ionization signal is composed of three different parts, ignition, flame front, and post flame, is the basis for the third algorithm. Since the flame front and post flame phases give the signal its characteristic appearance, it may be possible to construct an ideal model of the ionization signal from this information.

The three phases of the ionization signal are shown in Figure 3.8. The second phase, the flame front, has a high ionization current level associated with the flame. This high ionization current level decays quite quickly. As a result the flame front can be described as a peak which decays down to zero. The third phase, post flame, has an ionization current which, to some extent, follows the pressure.

It is appealing to look at the ionization signal as a sum of two signals, where the

first represents the flame front phase and the second the post flame phase. Since the pressure is shaped as a bulb, the part of the ionization connected to the pressure might also be shaped as a bulb. A model available by Mecel relates ionization current and pressure at thermodynamical equilibrium for the ions. This model is used to derive the signals in Figure 5.8. The dashed signal in the plot is an Gaussian function with the
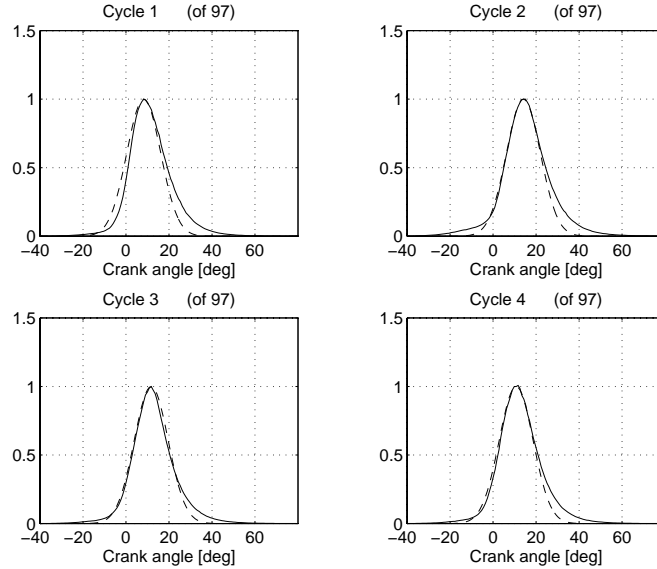
Figure 5.8. Pressure converted to ionization current for 3000 rpm, 90 Nm. Filled line is the pressure and dashed is the Gaussian function.

maximum equal to the maximum of the ionization signal retrieved from the pressure. The Gaussian function is described by,

$$f(\theta) = \alpha_1 e^{-\alpha_2(\theta - \alpha_3)^2}$$

As it can be seen the signals are similar. On this basis the function used for approximating the post flame phase is chosen as an Gaussian function.

The function for approximating the flame front phase is also chosen as a Gaussian function. The flame front is a high peak which is zero in the beginning and the end, and choosing the same function as for the post flame give similar parameters to estimate. There might exist other functions that are better approximations for these phases than two Gaussian functions. Since this is a study of the concepts, the functions used are as simple as possible.

The approximation should fit as close as possible to the ionization signal. A regular criterion is to minimize the square of the difference between the signals. The result is to minimize a least-square criterion, which is a well defined problem. This does not mean that the problem is easy to solve. Since the functions are non convex and non-linear, it is actually a quite difficult problem. A comprehensive explanation of the optimization algorithm and the implementation is given in Section 6.3.

6   Algorithm implementations

The implementation and a description of the algorithms is contained in this section. The algorithms are implemented in Matlab. The actual Matlab code is not cited, instead pseudocode for the algorithms is displayed. The reason is that Matlab code will hide the important parts of the algorithms in details specific for Matlab.

6.1   Ion peak algorithm

The basic idea for this algorithm was to use the second ionization peak as an approximation for the pressure peak. The first order derivative is used to find the local maxima, and if a second ionization peak does not exist then the inflexion point is used instead.

The first step is to smooth the ionization signal. The signal is low-pass filtered, in order to extract the slow variations of the ionization signal and to eliminate the high frequency noise. The smoothing filter used has degree 7, which is tested to give a signal where the first and second order derivatives not fluctuate too much. The filter is described in Appendix B.

The first and second order derivative is used to search the interesting point of the ionization signal and to compute them approximations are used. The first order derivative is computed with the difference approximation,

$$f'(\theta_i) = \frac{1}{2}\frac{f(\theta_{i+1}) - f(\theta_i)}{\theta_{i+1} - \theta_i} + \frac{1}{2}\frac{f(\theta_i) - f(\theta_{i-1})}{\theta_i - \theta_{i-1}} \tag{6.1}$$

Under the assumption that the difference in angle between the samples is constant,

$$\theta_{i+1} - \theta_i = constant \ (= \frac{1}{c} > 0)$$

this difference approximation produces a derivative without phase shift. The derivative can in this case be rewritten

$$f'(\theta_i) = c(f(\theta_{i+1}) - f(\theta_{i-1}))$$

Since it is only the zero crossing of the derivative that is interesting it is sufficient to study

$$f'(\theta_i) \propto f(\theta_{i+1}) - f(\theta_{i-1}) \tag{6.2}$$

Under the same circumstances and assumptions as above, the difference approximating for the second order derivative is

$$f''(\theta_i) \propto f(\theta_{i+1}) - 2f(\theta_i) + f(\theta_{i-1}) \tag{6.3}$$

In Section 5.2 it was mentioned that there is a trade-off between an early and a late search start, when searching for the post-flame peak. Since the pressure peak θ_{pp} does not appear earlier than $5°$ after TDC, the search is started at $5°$ after TDC. The interesting region is between crank angles $5°$ and $30°$, and therefore the search is made between these crank angles. If a maximum does not exist in this range the inflexion point is to be used, which is searched for in the same interval, $5°$ to $30°$.

It is possible that there does not exist an inflexion point in the interval. In such a case a default value is used instead. Also a moving average from the previous 5-30 cycles

could be used. In the data studied there always exists an inflexion point in the interval. Therefore the algorithm is not implemented with such a feature. If there exists a late peak from the flame front within 5° to 30°, the algorithm returns this point instead of the post flame maximum.

The characteristics for a maximum between θ_{i-1} and θ_i is that $f'(\theta_{i-1}) > 0$ and $f'(\theta_i) \leq 0$. For an inflexion point the condition is that $f''(\theta_{i-1}) > 0$ and $f''(\theta_i) \leq 0$. Consequently, such sign shifts are searched.

Implementation

The algorithm is as follows.

FOR every cycle **DO**
    BEGIN
        Smooth the signal
        Compute the first and second order derivatives
        (* Search the start index *)
        WHILE $\theta_i < 5°$ **DO**
            $i = i + 1$
        $start = i$
        (* Search for a maximum *)
        WHILE $\left\{ \text{not} \left((I'(\theta_i) \geq 0°) \; and \; (I'(\theta_{i+1}) < 0°) \right) \right\}$ and $\left\{ \theta_i \leq 30° \right\}$ **DO**
            $i = i + 1$
        (* Test if the point found is within the range *)
        IF $\theta_i > 30°$ **THEN**
            BEGIN
                $i = start$
                (* Search for an inflexion point *)
                WHILE$\left\{ \text{not} \left((I''(\theta_i) \geq 0°) \; and \; (I''(\theta_{i+1}) < 0°) \right) \right\}$ and $(\theta_i \leq 30°)$ **DO**
                    $i = i + 1$
        END
END

Improvements

The algorithm can be improved in several ways, to visualize this two proposals for improvements are shortly described. One is to start the search earlier, and first search an inflexion point and then a following maximum. If a maximum is not found in the interesting interval, then use the inflexion point previously found. This would eliminate some occurences when the algorithm gets stuck at a late peak in the flame-front. Another way is to perform the search of the ionization signal backwards. Such a search will find the latest peak in the ionization signal. The search still finds the flame front if it has long duration and the post flame does not have a peak.

6.2   Ion mass center

The basic idea for this algorithm is that the mass center of the post flame phase of the ionization current is a reflection of the pressure peak angle.

In order to get compact expressions in the algorithms it is convenient to introduce some notations. Let θ denote the crank angle relative to TDC, negative before and positive after TDC, and let S_θ denote the interesting part of the cycle to study, i.e. in most cases, crank angles between -30° and 60°. Let θ_i denote the crank angle to sample i, and S_i the subset of indices for the samples such that crank angle for these samples falls within the interesting interval S_θ, i.e. $S_i = \{i \mid \theta_i \in S_\theta\}$. The mass center is computed between the crank angles $-20°$ and $50°$, this gives $S_i = \{i \mid -20° \leq \theta_i \leq 50°\}$.

There are several different centroids that are interesting to examine, one example is to raise the signal to the power of 2, i.e. $f(\theta_i) = (I(\theta_i))^2$. This increases the difference between small and large values in $I(\theta)$, and the interpretation is that the mass center moves towards the maximum of the signal.

The mass center algorithm uses several different centroids, still these are basically computed in the same way. The centroid for a function, $f(\theta)$, is computed as follows

$$\frac{\int_{\theta \in S_\theta} \theta\, f(\theta)\, d\theta}{\int_{\theta \in S_\theta} f(\theta)\, d\theta} \tag{6.4}$$

The ionization signal is sampled and the computations are preformed on a time discrete signal. The definition of the centroid in the discrete case is analogous to the continuous case. Using the conventions above for the crank angle and the subset of samples the result is

$$\frac{\sum_{i \in S_i} \theta_i\, f(\theta_i)}{\sum_{i \in S_i} f(\theta_i)} \tag{6.5}$$

The angle at DP, discarding point, is denoted θ_{DP}. The search for θ_{DP} uses the second order derivative. Before the signal is derived it must be smoothed, because the second order derivative will else way be inflected by the noise. The smoothing filter is described in Appendix B. The search for the discarding point is started at $\theta = 0°$.

The first correction of the signal is to set the ionization signal equal to zero before θ_{DP}. One example is displayed in Figure 5.6.

As a second alternative correction a line is fitted to the derivative of the signal at θ_{DP}, which is explained in Figure 5.6. The signal before θ_{DP} is replaced by a line which has the same derivative as the ionization signal at θ_{DP}. To derive the equation for this correction, the constraints must be noted. The first constraint is that the derivatives, at θ_{DP}, of the signal and the corrected signal should be equal. The second constraint is, that the corrected signal must be continuous at θ_{DP}. If the corrected signal is denoted, $C(\theta)$, the constraints are

$$\begin{cases} I(\theta_{DP}) & = & C(\theta_{DP}) \\ I'(\theta_{DP}) & = & C'(\theta_{DP}) \end{cases}$$

This gives the equation for the correction

$$C(\theta) = I'(\theta_{DP})(\theta - \theta_{DP}) + I(\theta_{DP}) \tag{6.6}$$

For the implementation of this correction it is interesting to know at what crank angle, θ_z, the correction, $C(\theta)$, is zero. Some manipulating with Equation (6.6) give

$$\theta_z = \theta_{DP} - \frac{I(\theta_{DP})}{I'(\theta_{DP})}$$

The third alternative for a correction is also shown in Figure 5.6. It is a parable which has to fulfil three criterions:

- The derivative of the parable must be equal to the derivative of the ionization signal at θ_{DP}.

- The signal value at θ_{DP} must be the same for both the ionization and the correction.

- The parable must decrease down to zero, and have the minimum there. The crank angle at the minimum is called θ_z.

The third constraint gives the equation for the parable as

$$C(\theta) = k(\theta - \theta_z)^2 \ , \ k > 0 \tag{6.7}$$

The first constraint together with the Equation (6.7) give

$$I'(\theta_{DP}) = 2k(\theta_{DP} - \theta_z) \tag{6.8}$$

Finally the second constraint together with Equation (6.7) give

$$I(\theta_{DP}) = k(\theta_{DP} - \theta_z)^2 \tag{6.9}$$

The two Equations (6.8) and (6.9), give a system of two equations with two unknown variables k and θ_z, and the solution is

$$\begin{cases} \theta_z &= \theta_{DP} - 2\frac{I(\theta_{DP})}{I'(\theta_{DP})} \\ k &= \frac{I'(\theta_{DP})}{2(\theta_{DP} - \theta_z)} \end{cases}$$

The problem that the derivative of I, at θ_{DP}, may be too small or negative remains. This is overcome by testing if $I'(\theta_{DP}) \leq smallvalue$ and then setting $I'(\theta_{DP})$ to a default value. The new $I'(\theta)$ is then used for the computation of the corrections.

If θ_z is set equal to θ_{DP} for the first correction, the three different algorithms can use the same pseudocode.

Implementation

The pseudocode for the algorithm is as follows

FOR every cycle **DO**
    BEGIN
        Smooth the signal
        Compute the first and second order derivatives
        Initialize $i = 0$
        (* Search the start index *)

    WHILE $\theta_i < 0°$ **DO**
       $i = i + 1$
    (* Search for a inflexion point *)
    WHILE $\left\{ \text{ not } \left((I''(\theta_i) \geq 0°) \ and \ (I''(\theta_{i+1}) < 0°) \right) \right\}$ and $\left\{ \theta_i \leq 30° \right\}$ **DO**
       $i = i + 1$
    (* Compute the parameters for the corrections *)
    θ_z, k, and $I'(\theta)$
    (* Compute the correction $I_c(\theta)$ *)
    Initialize $i = 0$
    WHILE $\theta_i < \theta_z$ **DO**
       BEGIN
          $I_c(\theta_i) = 0$
          $i = i + 1$
       END
    WHILE $\theta_i < \theta_{DP}$ **DO**
       BEGIN
          $I_c(\theta_i) = C(\theta_i)$
          $i = i + 1$
       END
    WHILE $i \in S_i$ **DO**
       BEGIN
          $I_c(\theta_i) = I(\theta_i)$
          $i = i + 1$
       END
END

From this algorithm the corrected ionization signal, $I_c(\theta)$, is returned. This signal is used as input to the algorithm for computing the mass center. Before the mass center is computed the value for the power p must be determined. The algorithm is then as follows

FOR every cycle **DO**
   BEGIN
     (* Search the start index *)
     $i = 0$
     WHILE $i \notin S_i$ **DO**
       $i = i + 1$
     $start = i$
     (* Compute the function $f(\theta)$ *)
     WHILE $i \in S_i$ **DO**
       BEGIN
          $f(\theta_i) = (I_c(\theta_i))^p$
          $i = i + 1$
       END
     $i = start$
     $Sum_1 = 0$
     $Sum_2 = 0$

```
(* Compute the sums *)
WHILE i ∈ S_i DO
    BEGIN
        Sum_1 = Sum_1 + θ_i f(θ_i)
        Sum_2 = Sum_2 + f(θ_i)
        i = i + 1
    END
(* Compute the mass center *)
Q = Sum_1/Sum_2
END
```

6.3 Ion structural analysis

The ionization signal consists of three phases where the two last phases are extracted by an algorithm that fits a model of the ideal ionization signal to the measured.

The model of the ionization signal is two Gaussian functions. The mathematical description of a Gaussian function is

$$f(\theta) = \alpha_1 e^{-\alpha_2(\theta - \alpha_3)^2}$$

The parameters, α_1, α_2, and α_3 changes the shape of the function. α_1 changes the height, α_2 affects the width, and α_3 is the position for the center.

Denote the measured ionization signal with $I(\theta)$ and the Gaussian functions $f_1(\theta)$, $f_2(\theta)$ then the model is $I(\theta) \approx f_1(\theta) + f_2(\theta)$ where $f_1(\theta)$ and $f_2(\theta)$ are

$$f_1(\theta) = \alpha_1 e^{-\alpha_2(\theta - \alpha_3)^2}$$
$$f_2(\theta) = \beta_1 e^{-\beta_2(\theta - \beta_3)^2}$$

As mentioned before the least square fit is used. The interpretation is to minimize the energy of the error between the model and the ionization signal. The error function is

$$err(\theta) = I(\theta) - f_1(\theta) - f_2(\theta) \tag{6.10}$$

The minimization is performed over the interesting interval, S_i. The signal is sampled values at the points θ_i, where i denotes the sample number. This corresponds to minimization of the loss function

$$, = \sum_{i \in S_i} (err(\theta_i))^2$$

with respect to the six parameters α_1, α_2, α_3, β_1, β_2, and β_3. The criterion , is with (6.10) inserted

$$, (\alpha_1, \alpha_2, \alpha_3, \beta_1, \beta_2, \beta_3) = \sum_{i \in S_i} (I(\theta_i) - \alpha_1 e^{-\alpha_2(\theta_i - \alpha_3)^2} - \beta_1 e^{-\beta_2(\theta_i - \beta_3)^2})^2 \tag{6.11}$$

Some intuitive constraints are applied to the problem. At first the constraint

$$\alpha_3 \leq \beta_3 \tag{6.12}$$

must be valid, in order to hold the signal $f_1(\theta)$ to the flame front which appears earlier than the post flame corresponding to $f_2(\theta)$. This constraint is not necessary to evaluate during the optimization, instead it is possible to test it after the optimization is finished and then exchange the functions. Next constraints are,

$$\alpha_2 > 0 \qquad\qquad (6.13)$$
$$\beta_2 > 0 \qquad\qquad (6.14)$$

these makes the functions look like a Gaussian function.

Analytical solution for two parameters

This is a difficult optimization problem since the functions are non-linear and non-convex. Though, it is possible to solve the problem for two parameters analytically, i.e the parameters α_1 and β_1. This reduces the number of parameters for the optimization algorithm to "only" four. The calculus for this reduction is presented below.

The partial derivative of the loss function , with respect to α_1 and β_1 is,

$$\frac{\partial ,}{\partial \alpha_1} = -2 \sum_{i \in S_i} (I(\theta_i) - \alpha_1 e^{-\alpha_2(\theta_i-\alpha_3)^2} - \beta_1 e^{-\beta_2(\theta_i-\beta_3)^2}) e^{-\alpha_2(\theta_i-\alpha_3)^2}$$

$$\frac{\partial ,}{\partial \beta_1} = -2 \sum_{i \in S_i} (I(\theta_i) - \alpha_1 e^{-\alpha_2(\theta_i-\alpha_3)^2} - \beta_1 e^{-\beta_2(\theta_i-\beta_3)^2}) e^{-\beta_2(\theta_i-\beta_3)^2}$$

For a stationary point the criterion $\frac{\partial \Gamma}{\partial \alpha_1} = 0$ and $\frac{\partial \Gamma}{\partial \beta_1} = 0$ must be fulfilled. This is a system of two equations that can be solved for α_1 and β_1. It can be rewritten as

$$\alpha_1 \sum_{i \in S_i} (e^{-\alpha_2(\theta_i-\alpha_3)^2})^2 + \beta_1 \sum_{i \in S_i} e^{-\alpha_2(\theta_i-\alpha_3)^2} e^{-\beta_2(\theta_i-\beta_3)^2} = \sum_{i \in S_i} I(\theta_i) e^{-\alpha_2(\theta_i-\alpha_3)^2}$$

$$\alpha_1 \sum_{i \in S_i} e^{-\alpha_2(\theta_i-\alpha_3)^2} e^{-\beta_2(\theta_i-\beta_3)^2} + \beta_1 \sum_{i \in S_i} (e^{-\beta_2(\theta_i-\beta_3)^2})^2 = \sum_{i \in S_i} I(\theta_i) e^{-\beta_2(\theta_i-\beta_3)^2}$$

Let this set of equations be equal to

$$\alpha_1 A + \beta_1 B = D$$
$$\alpha_1 B + \beta_1 C = E$$

where

$$A = \sum_{i \in S_i} (e^{-\alpha_2(\theta_i-\alpha_3)^2})^2, B = \sum_{i \in S_i} e^{-\alpha_2(\theta_i-\alpha_3)^2} e^{-\beta_2(\theta_i-\beta_3)^2}, C = \sum_{i \in S_i} (e^{-\beta_2(\theta_i-\beta_3)^2})^2$$

$$D = \sum_{i \in S_i} I(\theta_i) e^{-\alpha_2(\theta_i-\alpha_3)^2}, E = \sum_{i \in S_i} I(\theta_i) e^{-\beta_2(\theta_i-\beta_3)^2}$$

The solution is

$$\alpha_1 = \frac{CD - BE}{CA - B^2}, \qquad \beta_1 = \frac{AE - BD}{CA - B^2} \qquad\qquad (6.15)$$

The last thing to verify is whether or not this stationary point is a minimum or not. A local minimum is characterized by a positive second order derivative. The second order derivative of , with respect to α_1 and β_1 is as follows

$$\frac{\partial^2 ,}{\partial \alpha_1^2} = 2 \sum_{i \in S_i} (e^{-\alpha_2 (\theta_i - \alpha_3)^2})^2 > 0$$

$$\frac{\partial^2 ,}{\partial \beta_1^2} = 2 \sum_{i \in S_i} (e^{-\beta_2 (\theta_i - \beta_3)^2})^2 > 0$$

Numerical solution for four parameters

For each value of the parameters α_2, α_3, β_2 and β_3 it is possible to compute the parameters α_1 and β_1. Hence, the optimization algorithm only needs to concentrate on four variables instead of six.

The optimization algorithm chosen is a gradient algorithm [9]. If the problem is convex, the algorithm converges towards the optimum. In this case the problem is non-convex which bring about that the algorithm might converge towards a local optima. It is, to some extent, possible to avoid that the algorithm finds a bad local minimum. Since the algorithm is iterative it will need an initial guess of solution, the better this first guess is the quicker the algorithm finds a good solution. If the initial guess is close to global optimum the algorithm will converge towards it. Hence, it is preferable to give the algorithm a good initial guess.

The first Gaussian function represents the flame front peak. Therefore α_3 is set equal to the ionization peak. The second signal represents the post-flame peak, which does not always exist, therefore it is not possible to search for the second peak. The difference between the peaks is normally $17°$ and consequently β_3 is set to $\alpha_3 + 17°$. The parameters α_2 and β_2 are set to normal values for the functions, i.e. $\alpha_2 = 0.01$ and $\beta_2 = 0.002$. This is a heuristic for an initial guess that always will provide a feasible solution for the algorithm.

Since the algorithm uses the gradient, the partial derivatives of , has to be computed.

$$\frac{\partial ,}{\partial \alpha_2} = 2 \sum_{i \in S_i} (I(\theta_i) - \alpha_1 e^{-\alpha_2 (\theta_i - \alpha_3)^2} - \beta_1 e^{-\beta_2 (\theta_i - \beta_3)^2}) \alpha_1 e^{-\alpha_2 (\theta_i - \alpha_3)^2} (\theta_i - \alpha_3)^2$$

$$\frac{\partial ,}{\partial \beta_2} = 2 \sum_{i \in S_i} (I(\theta_i) - \alpha_1 e^{-\alpha_2 (\theta_i - \alpha_3)^2} - \beta_1 e^{-\beta_2 (\theta_i - \beta_3)^2}) \beta_1 e^{-\beta_2 (\theta_i - \beta_3)^2} (\theta_i - \beta_3)^2$$

$$\frac{\partial ,}{\partial \alpha_3} = -4 \sum_{i \in S_i} (I(\theta_i) - \alpha_1 e^{-\alpha_2 (\theta_i - \alpha_3)^2} - \beta_1 e^{-\beta_2 (\theta_i - \beta_3)^2}) \alpha_1 e^{-\alpha_2 (\theta_i - \alpha_3)^2} \alpha_2 (\theta_i - \alpha_3)$$

$$\frac{\partial ,}{\partial \beta_3} = -4 \sum_{i \in S_i} (I(\theta_i) - \alpha_1 e^{-\alpha_2 (\theta_i - \alpha_3)^2} - \beta_1 e^{-\beta_2 (\theta_i - \beta_3)^2}) \beta_1 e^{-\beta_2 (\theta_i - \beta_3)^2} \beta_2 (\theta_i - \beta_3)$$

This gives the gradient ξ for , as,

$$\xi = \begin{pmatrix} \frac{\partial \Gamma}{\partial \alpha_2} \\ \frac{\partial \Gamma}{\partial \beta_2} \\ \frac{\partial \Gamma}{\partial \alpha_3} \\ \frac{\partial \Gamma}{\partial \beta_3} \end{pmatrix} \tag{6.16}$$

Some parameters must be initialized before the algorithm is started. These are: n_{max} a maximum number of iterations, ϵ a small value for the loss function, LBD lower bound to the loss function, UBD, upper bound for the loss function.

Let ξ_n denote the gradient ξ in step n, and let x_n denote the vector

$$x_n = \begin{pmatrix} \alpha_2 \\ \beta_2 \\ \alpha_3 \\ \beta_3 \end{pmatrix}$$

with the values of α_2, α_3, β_2, and β_3 in step n.

Implementation

The pseudocode for the optimization algorithm is
FOR every cycle **DO**
    BEGIN
        (* Find an initial guess, x_1 *)
        Search maximum for the ionization current, θ_{max}
        $\alpha 3 = \theta_{max}$, $\beta_3 = \theta_{max} + 17°$, $\alpha_2 = 0.01$, $\beta_2 = 0.002$
        (* Initialize the optimization algorithm *)
        $UBD = \infty$, $LBD = 0$, $stop = false$
        $n = 1$
        REPEAT
            Compute α_1 and β_1 from (6.15)
            Compute ξ_n and , from (6.16) and (6.11)
            IF , $< UBD$ **THEN**
                BEGIN
                    Save the current solution as best
                    $UBD = ,$
                END
            (* Test if stop *)
            IF $(|\xi_n| = 0)$ or $(, < \epsilon)$ or $(n > n_{max})$ **THEN**
                $stop = true$
            (* compute the step length, t, and the new x_{n+1} *)
            $t = \dfrac{\Gamma - LBD}{\|\xi_n\|^2 \left(1 + \frac{n}{10}\right)}$
            $x_{n+1} = x_n - t\xi_n$
            (* Test the constraints (6.13) and (6.14) *)
            IF $(\alpha_2$ in $x_{n+1}) < 0$ **THEN**
                Set α_2 to the previous value in x_n
            IF $(\beta_2$ in $x_{n+1}) < 0$ **THEN**
                Set β_2 to the previous value in x_n
            $n = n + 1$
        UNTIL $stop = true$
        (* Test the constraint (6.12) *)
        IF $\alpha_3 > \beta_3$ **THEN**
            BEGIN
                (* Exchange the Gaussian functions *)
                $\alpha_1 \longleftrightarrow \beta_1$

$$\alpha_2 \longleftrightarrow \beta_2$$
$$\alpha_3 \longleftrightarrow \beta_3$$

END

END

This algorithm stops after maximum n_{max} steps, due to the test criterion. It might stop earlier if either the gradient or the loss function becomes small enough. In most cases the algorithm iterates until the maximum number of iterations has been reached.

7 Algorithm results

The ignition timing during the measurements is constant, therfore the variations in the pressure and ionization signal are due to only the cycle to cycle variations.

The results are presented for the operating points with engine speed 3000 *rpm*. The reason is, as commented in Section 4.4, that the signals for the operating points at 4500 *rpm*, is similar to the operating points at 3000 *rpm*. The datasets are similar and hence the results are almost identical.

Two measures are used for comparing the results between the algorithms. The measures compare the values from the algorithms with the actual pressure peak, and computes a quantity that reflects the error in some way. The main reason for using a measure is that it give a quantity which can be compared. The measures does not provide an exact measure for the performance of the methods, therfore the measures are not perfect performance meters of the algorithms. However, there might exist other measures that reflects the properties better than the ones used in this study. The main objective is to study the three algorithms and their behavior, therefore the measures are not studied in detail. The measures are described more closely in Section 7.1.

7.1 Ion peak algorithm

Figure 7.1 shows six consecutive cycles with the ionization current plotted together with the points computed by the algorithm. This figure shows just that the algorithm returns expected values. It must be noted that the peak is searched on the ionization signal after it has been smoothed. Therfore, the points returned are not the first small local maxima after the search starts. Instead a larger maxima is retrieved.
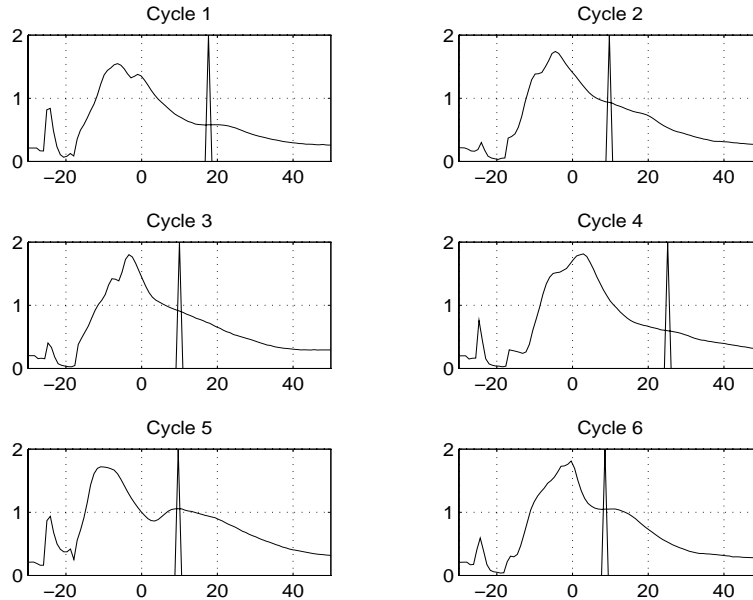

Figure 7.1. Ionization current and the point found by the ion peak algorithm. The operating point is 3000 rpm and 50 Nm for this plot.

The Figure 7.2 shows a correlation plot (a plot where the values from the same cycle are plotted together) between the position for the pressure peak and the point computed

by the ion peak algorithm. It is not possible to see if there exists a strong correlation between the pressure peak and the ionization peak found by the algorithm.
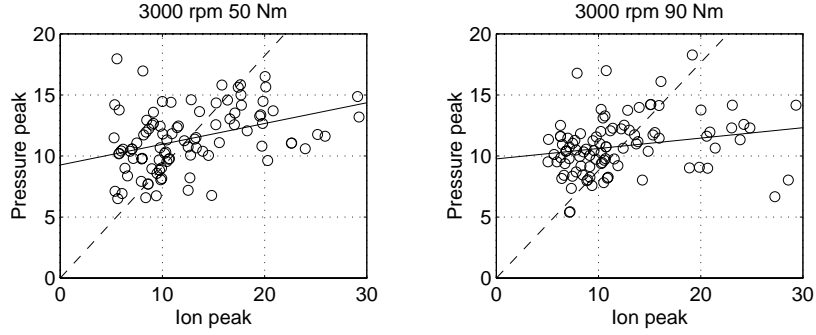

Figure 7.2. Ion peak plotted compared with pressure peak.

The measures M_1 and M_2

Basically the measures fit a line between the pressure and the points returned from the algorithms, and the deviation from the lines is the measure. The first measure is derived from a line through the origin in the plot. This line is fitted, in least squares meaning, to the points in the plot. This is equal to minimize, S_1 in Equation (7.1), with respect to l. Let i denote the cycle number, $PP(i)$ the peak pressure at cycle i, $IP(i)$ the ion peak at cycle i. Then S_1 is

$$S_1 = \sum_{i=1}^{N} (PP(i) - l * IP(i))^2 \tag{7.1}$$

The solution to this minimization problem is

$$l = \frac{\sum_{i=1}^{N} PP(i)}{\sum_{i=1}^{N} IP(i)}$$

The line from this fit is displayed as a dashed line in Figure 7.2. The measure is the mean square of the error, i.e. $M_1 = \frac{S_1}{N}$, which corresponds to the variance of difference from the line.

The motive for this fit and measure, is that the point derived from the ionization signal is an approximation for the pressure peak. This line has one degree of freedom, instead of just a straight line with fixed l (e.g. $l = 1$). Since the ionization peak is not equal to the pressure peak the slope, l, might take care of some connection that exists between the ionization and the pressure.

The second measure also involves the least squares fit of a line, in this case the line has two degrees of freedom. The line is not forced through the origin, instead it is free to move over the plot. This give the function the following appearance, $PP(i) = k * IP(i) + m$. The minimization problem is in this case,

$$S_2 = \sum_{i=1}^{N} (PP(i) - k * IP(i) - m)^2 \tag{7.2}$$

This is a well known mathematical problem, and the solution is described in e.g. [15]. In Figure 7.2 the fitted line is displayed as a filled line. In this case the measure is also

the mean square of the error, i.e. $M_2 = \frac{S_2}{N}$. The motive for this measure is analogous to the earlier described.

In Table 7.1 the values for l, k, m, M_1 and M_2 for the fit are shown. One thing

Engine speed (rpm)	Engine load (Nm)	l	k	m	M_1	M_2
3000	50	0.91	0.17	9.26	23.20	5.58
3000	90	0.88	0.09	9.76	27.96	5.10

Table 7.1. k and m for the fit of a line.

that is interesting to note, is that the values of M_1 and M_2 differs quite a lot. This is of course natural since the fit associated with M_2 has an additional degree of freedom.

Another notable thing is that l is quite near 1 and that k is much smaller.

7.2 Ion mass center

In this section the results from the mass center algorithms are descried. The structure of the presentation of the results is the same as in the earlier Section 7.1. It begin with a plot of the points found by the algorithm together with the ionization signal itself. Then the correlation plot is shown, and last a table of the measures and the values of the parameters in the fit.

In Figure 7.3 the points that the algorithm return, is plotted together with the ionization signal itself. This plot shows that the algorithm which computes the mass center of the non-corrected ionization signal, returns the real mass center (or centroid).
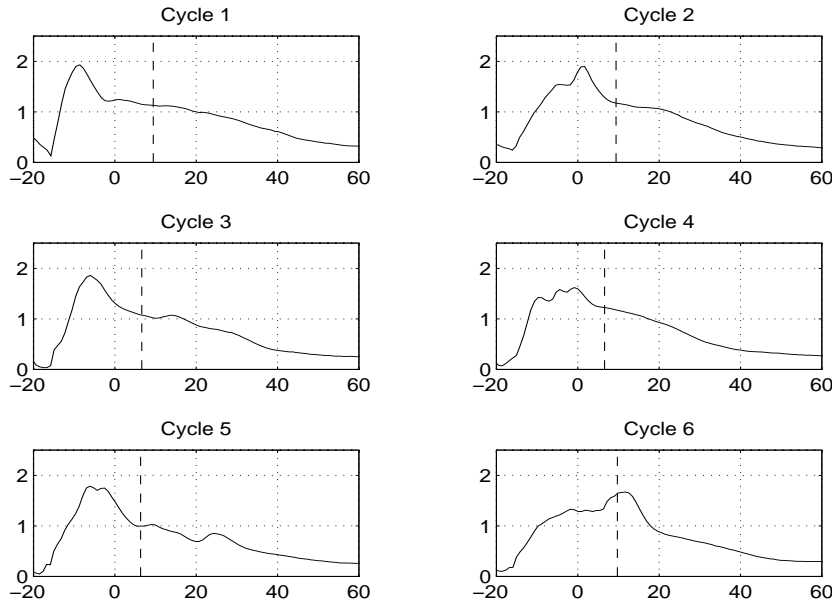

Figure 7.3. Mass center for a non corrected signal together with the ionization signal.

The plot shows that the mass center algorithm works, and finds the centroid of the ionization signal. This plot is the only one showing the points returned by the mass center algorithm together with the ionization signal. The variations of this algorithm

have other parameters, such as the DP, which inflect the computation of the mass centers. Therefore a plot showing the ionization signal and the mass center, for these refinements of the algorithm, does not show anything interesting.

A correlation plot between the mass center for a non corrected ionization signal and the pressure peak is displayed in Figure 7.4. As it can be seen there is not much correlation between the mass center and the pressure peak in these plots. The reason for this is that the flame-front of the ionization signal inflects the mass center of the ionization signal to much. A correlation plot between the mass center of an ionization
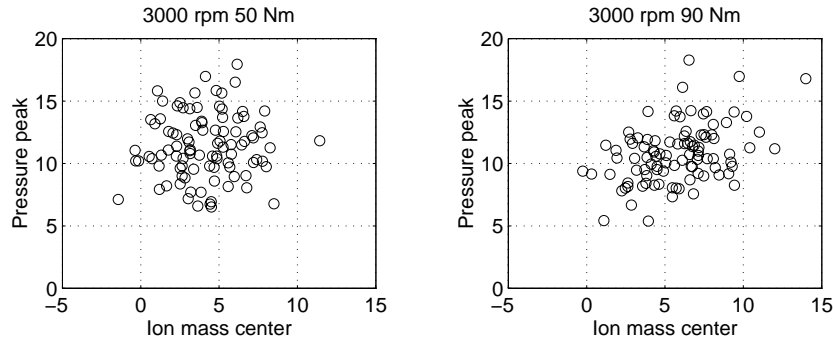

Figure 7.4. Mass center for a non corrected signal against the pressure peak. Note that the axis is differently scaled compared with the other plots.

signal which is cut-off, and the pressure peak is displayed in Figure 7.5. It is hard to see whether or not the mass center for this corrected ionization signal is connected to the pressure peak. The lines described earlier are also displayed in these figures. The parameters and the measures are shown in Table 7.2, together with the results from the other variations of the mass center algorithm.
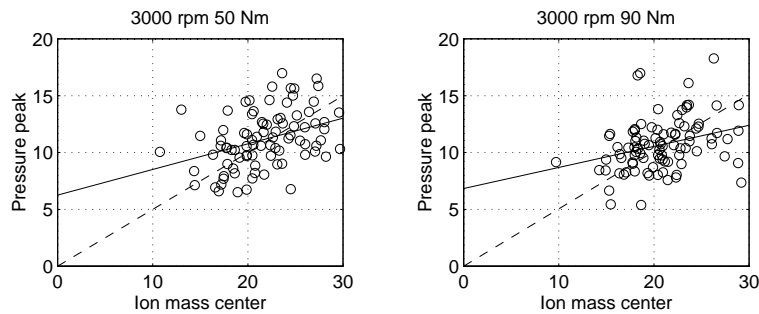

Figure 7.5. Mass center plotted against the pressure peak. The correction used is the first, i.e. cut-off.

Figure 7.6 displays a correlation plot between the mass center and the pressure peak, for this case. When the ionization signal is corrected with just a cut-off and then squared, i.e. exponent $p = 2$, the mass center moves towards the peak of the corrected signal. When the plots 7.5 and 7.6 are compared, this phenomena can clearly be seen. The mass center is positioned more to the left in the latter figure. The peak is positioned to the left of the centroid in the ionization signal that is cut-off. This behavior is repeated for higher exponents p.

In Figure 7.7 the exponent p is five. Here the mass centers have moved even more to the left, which is analogous to the above. The fitted lines are also displayed. In Table

Exponent p	Engine speed (rpm)	Engine load (Nm)	l	k	m	M_1	M_2
1	3000	50	0.50	0.22	6.25	7.15	5.16
1	3000	90	0.50	0.19	6.84	6.88	4.60
2	3000	50	0.57	0.22	6.98	8.89	4.92
2	3000	90	0.56	0.18	7.48	8.48	4.60
3	3000	50	0.62	0.22	7.38	10.46	4.85
3	3000	90	0.65	0.18	7.83	9.91	4.60
5	3000	50	0.66	0.21	7.75	12.51	4.81
5	3000	90	0.72	0.18	8.12	11.90	4.57

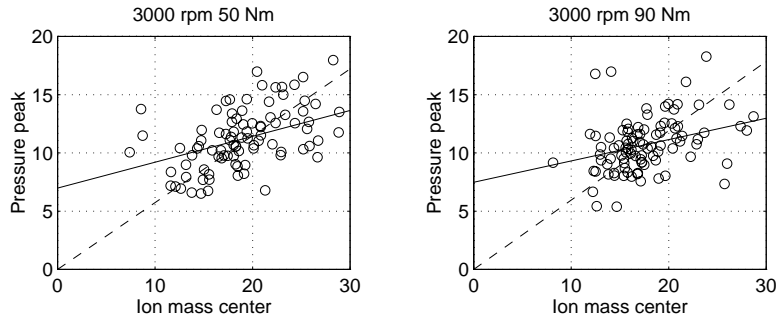**Table 7.2.** k, l, m and the measures for the fits.

Figure 7.6. Mass center for a corrected signal versus the pressure peak. ($p = 2$).

7.2 the values for the different parameters in the fit are shown.

The results from the algorithms with the corrections using a line and parable is almost identical to the results from the above described algorithms. The correction in these cases all use the same DP and the derivate is too small so it will be set to a default value. Since the corrections all get the default value which is the same for all cycles, the mass center is mainly depending on DP. This explains why the algorithms using the better corrections, return almost the same values as the algorithm with just a cut-off. On other ionization signals, which has appearances as described in the pre study, the corrections are of more importance for the mass center calculations. This since the corrections in these cases are dependant on DP as well as the derivative at DP.
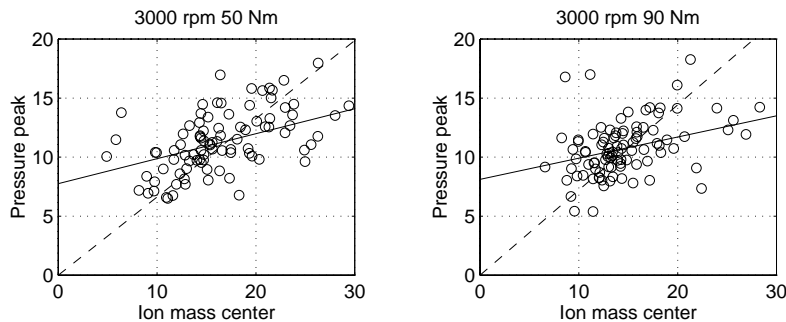

Figure 7.7. Mass center for a corrected signal versus the pressure peak. ($p = 5$).

The mass center is itself depending on the DP, Figure 7.8 displays a correlation plot between the computed mass center and DP. There exists a quite good correlation between the ionization mass center and DP, the connection is more strongly in the case with exponent $p = 2$.
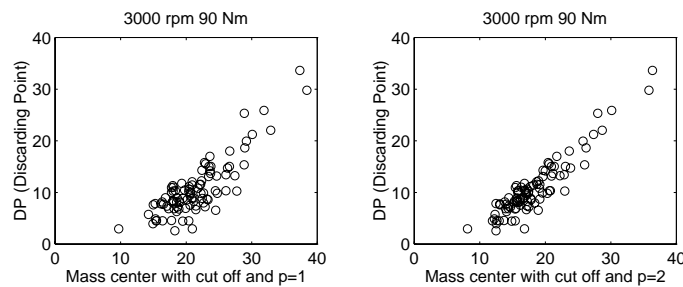

Figure 7.8. Ion mass center for a signal that is cut off, plotted against DP.

7.3 Ion structural analysis

Six ionization signals are displayed together with the fitted signals in Figure 7.9. As it can be seen in the figure the algorithm, for positioning the sum of the the Gaussian functions, work and produces a good fit.
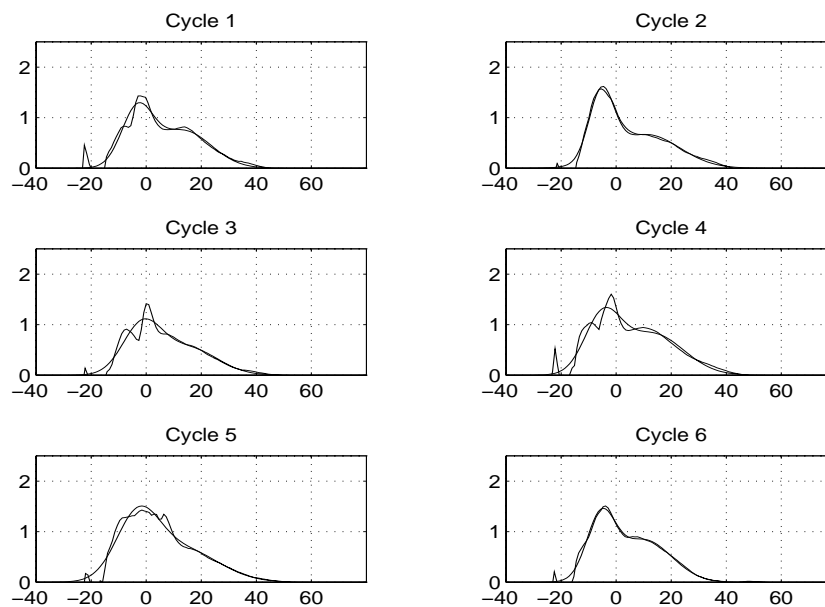
Figure 7.9. Plot of the fitted signal together with the ionization signal.

In Figure 7.10 the two gauss functions, that are components of the fitted signal, are plotted. The idea that the second signal would be fitted to the post-flame phase, seems to work quite well when studying the figure.

The connection between the second Gaussian signal and the pressure is interesting. A plot shown in Figure 7.11 displays these signals. The second signal extracted from the ionization signal correlates well with the position for the pressure. Some deviations between the pressure and the second signal are present, especially in cycles two and
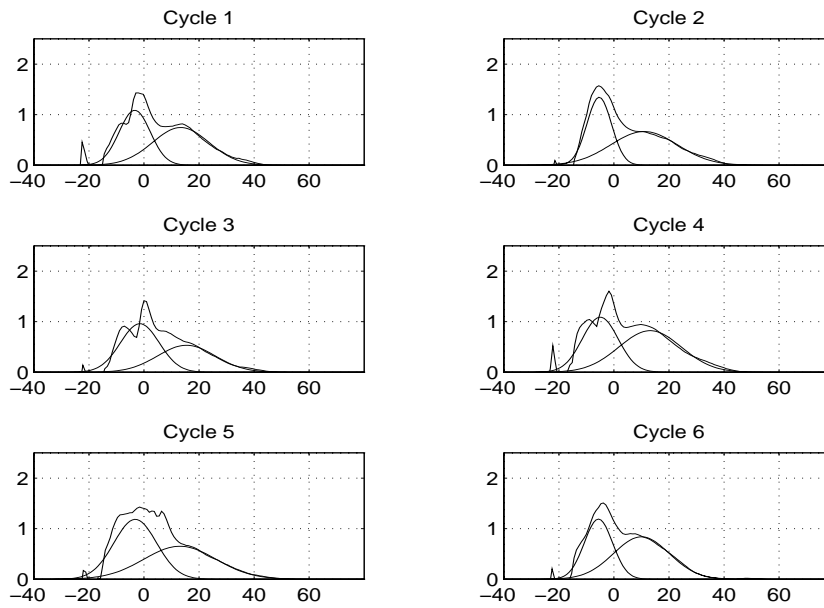
Figure 7.10. Plot of the fitted parts together with the ionization signal.
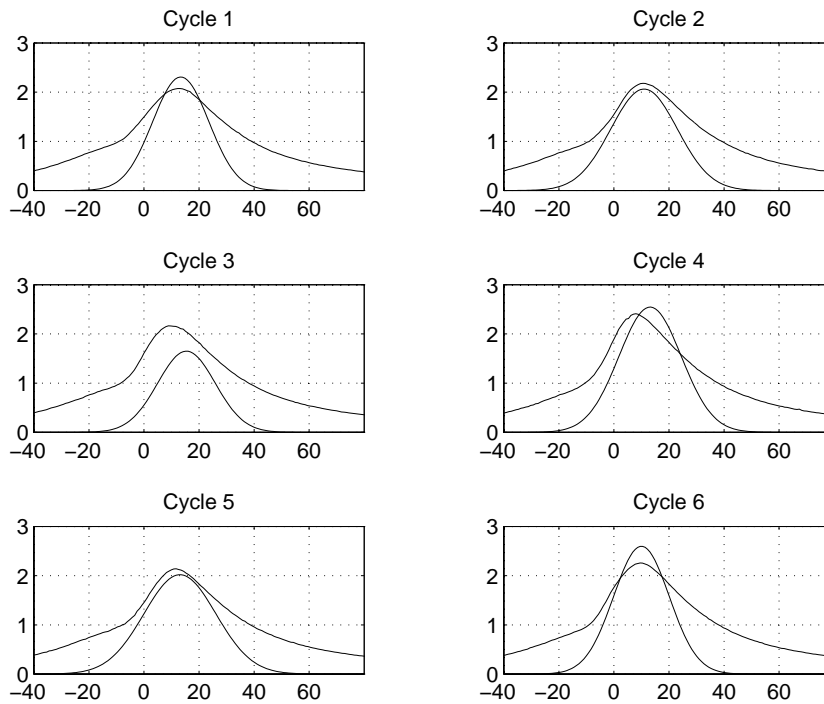
Figure 7.11. The pressure and the second Gaussian signal, the Gaussian signal scaled with a factor 3 for comparing.

three. In these cycles the ionization signals, displayed in Figure 7.9 have a large flame front. Hence it is possible to use the distorted flame front as a criterion for selecting what ionization signals that can be used.

In Figure 7.12 the position for the second peak is plotted against the pressure peak, the fitted lines are also displayed in the same plot. The values for the fitted lines and the

Figure 7.12. Plot of the second signal relative the pressure peak.

associated measures are shown in Table 7.3. One problem with this algorithm, for the time being, is that the optimization algorithm is slow because it has to iterate several times during the fitting procedure.

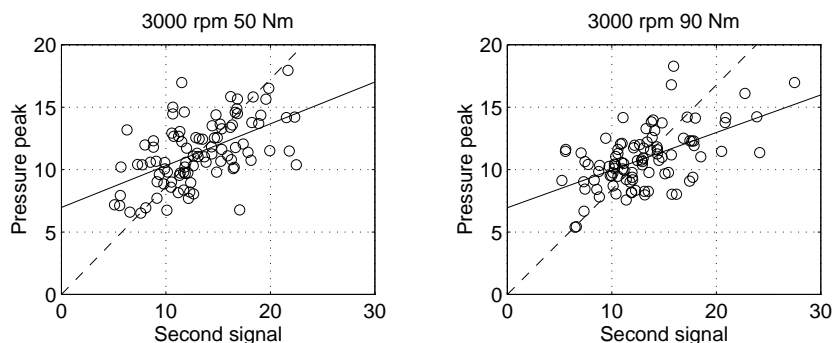| Engine speed (rpm)	Engine load (Nm)	l	k	m	M_1	M_2
3000	50	0.86	0.33	6.96	9.31	4.62
3000	90	0.84	0.30	6.94	8.83	3.68

Table 7.3. k and m for the fit of a line to a corrected signal. $p = 1$

7.4 Algorithm comparison

It is difficult to quantify the results and to compare the results from different algorithms, especially when they are based upon different ideas. Since there is not a perfect correlation between the points returned from the algorithms and the peak pressure, it is difficult to say anything definite about the test results. The measures compare the values from the algorithms with the actual pressure peak. The main reason for using a measure is that it gives a quantity which can be compared for the algorithms. However, there might exist other measures that reflects the properties better than the ones used in this study.

The ion peak algorithm follows the appearance of the signal and have problems with a long flame front and a post flame without a peak. The mass center algorithm use more information from the ionization signal, but the mass center is to a large extent depending on DP (Discarding Point). This makes the mass center depend on the ionization signals appearance. The ion structure analysis algorithm provide promising results and it is interesting to continue and study it.

The measures produce values which does not differ by magnitudes. Except for M_1 in the ion peak algorithm, the measures are quite equal. There are no big differences between the algorithms, which is mainly due to the constant ignition timing during the measurements. The variations retrieved in the pressure and ionization currents are due to cycle to cycle variations, which might be one reason for why the correlation plots does not give a better correlation.

The main results from the algorithms are summarized below.

- Ion peak

  This algorithm has several problems. First there is the point for the search start, if the flame front phase has long duration the algorithm returns a point from this phase. The next problem is when the post flame phase does not have a clear peak, in that case the algorithm use the inflexion point. It is questionable whether or not the inflexion point is correlated with the pressure peak. Generally the problem is that the algorithm is based upon the local behavior of the ionization signal. Since the ionization signal fluctuates a lot the algorithm follows these fluctuations. M_1 is large compared with the same measure for the other algorithms. If M_1 and k are compared to the values for the other algorithms, it can be seen that the point found is less correlated with the pressure peak.

- Ion mass center

  The mass center algorithm give promising results when the ionization signal has a very clear post flame phase. In the pre study the ionization signals have large post flame phases and the results there are promising. The mass center algorithm use more information about the ionization signal, than the ion peak algorithm, therefore it produces more stable results. When the ionization signal has a relatively large flame front the mass center algorithm is dependant of the DP (discarding point). The DP depends on the second order derivative of the signal which give the same problem as earlier, i.e. the ionization signal fluctuates and affects the DP which influences also the mass center to fluctuate.

- Ion structural analysis

  This algorithm produces promising results regarding the connection between the pressure and the second Gaussian signal. The optimization algorithm for positioning the Gaussian signals is time consuming. Therefore, it is not possible to implement the current version of this algorithm today in a real time application. Again it must be noted that it is only the behavior of the idea, to fit a model to the ionization signal, that is tested and not the efficiency of the optimization algorithm.

7.5 Future problems

When the sparkplug is used as ionization sensor the implementation of adjustable spark duration might be a problem for the measurement of ionization current. Since the spark, in some timing cases, might last into the interesting parts of the ionization signal it will disturb the measurement of the ionization current. A conflict between ignition timing and ionization measurement is apparent. In most cases the timing will not cause any problems but in some special cases information might be lost. A separate sensor is not affected by variable spark length, but then there are the problems of mounting an extra sensor.

7.6 Future extensions

There are several possible extensions to this work, some of them are presented below. The most interesting extension is to vary the ignition timing and test the algorithms on the new data sets. Since varied ignition timing changes the pressure characteristics,

more modes than the cycle to cycle variations can be studied. Such a test might show more clearly which algorithms that produces the best tracing of the pressure as well as the ignition timing.

In the ion peak algorithm, the zero crossings of the first and second order derivatives are studied together. If the cycles, where a maximum is found, are separated from the cycles where the inflexion point is used, different results might be received for the decomposed parts of this algorithm. The inflexion point could be studied more closely in such a test.

The mass center algorithm have problems with the flame front phase and depends to a large extent on the selection of DP (discarding point). Therefore, it is interesting to study if it is possible to choose another DP, which makes the mass center more independent of the ionization signal appearance.

In the ionization structure analysis the first Gaussian signal is fit to the flame front phase, merely to dispose the flame front and retrieve the post flame phase. Though, the flame ionization contains information about the combustion as well, and it might be possible to extract useful information from the first signal too.

The λ value affects the ionization signal and especially the flame front phase. The slope of the ionization signal in the flame front phase, corresponding to the frequency component of the flame front phase, contains information of the lambda value [13]. It is therefore interesting to examine the properties of the first Gaussian function and compare it with the λ value.

The optimization procedure in the ion structural algorithm is time consuming. Therefore, it is interesting to study if there exists other, more efficient, algorithms that solve the optimization problem.

8   Conclusions

The ionization signal contains information about several parameters which are important for the combustion. Aiming at controlling the work produced, three different algorithms for extracting information from the ionization signal have been studied: ion peak, ion mass center, and ion structural analysis. The algorithms are based upon different aspects of the ionization signal, and have their own characteristics.

The differences between the algorithms are not significant, which is mainly due to that ignition timing is not changed during the measurements. The variations in pressure peak and ionization currents received during the measurements are due to cycle to cycle variations in these processes.

The ion peak algorithm has several problems, generally the problem is that the algorithm is based upon the local behavior of the ionization signal. Since the ionization signal varies quite a lot, the algorithm "follows" these fluctuations. The main problems are: (1) the ionization signal does not have distinct position where the flame front phase shifts to the post flame phase; (2) the flame front lasts into the interesting parts of the signal and disturbs the algorithm; (3) the post flame phase does not have a distinct peak, and another point must be used instead.

The mass center algorithm use more information, than the ion peak algorithm, about the ionization signal, therefore it produces more stable results. In the pre study the ionization signals have relatively large post flame phases, and for these signals the mass center algorithm provides promising results. Though, it is important to comment that the data sets were small in this case. When the flame front is relatively large, the mass center algorithm depends on the DP (discarding point). Hence the mass center depends on the ionization appearance.

The ion structure analysis algorithm produces promising results regarding the connection between the pressure and the second Gaussian signal. The implemented optimization algorithm for retrieving a least square fit is time consuming, and is in its present form not suitable to implement in a real time system. Future studies will be performed on this algorithm since the results are promising.

References

[1] Robert L. Andersson. In-cylinder measurement of combustion characteristics using ionization sensors. *SAE Technical Paper Series*, 1986.

[2] V. Arrigoni, F. Calvi, G. M. Cornetti, and U. Pozzi. Turbulent flame structure as determined by pressure development and ionization intensity. *SAE Technical Paper Series*, 1973.

[3] AVL. *Operating Instructions: AVL 8 QP Quartz Pressure Transducers*, march 1987 edition, march 1987.

[4] AVL. *Operating manual: 3056-A01 Charge amplifier*, june 1991 edition, june 1991.

[5] K. N. C. Bray and N. Collings. Ionization sensors for internal combustion engine diagnostics. *Endeavour,New Series*, 15(1), 1991.

[6] Nick Collings, Steve Dinsdale, and Tim Hands. Plug fouling investigations on a running engine - an application of a novel multi-purpose diagnostic system based on the spark plug. *SAE Technical Paper Series*, 1991.

[7] P. Gillbrand, H. Johansson, and J. Nytomt. Method and arrangement for detecting ionising current in an internal combustion engine ignition system. EP, C, 188180, December 19 1994.

[8] John B. Heywood. *Internal Combustion Engine Fundamentals*. McGraw-Hill series in mechanical engineering. McGraw-Hill, 1992.

[9] Kaj Holmberg. *Primal and Dual Decomposition Methods and Search Methods: Introduction*. Optimeringslära, September 1992.

[10] M. Krämer and K. Wolf. Approaces to gasoline engine control involving the use of ion current sensory analysis. *SAE Technical Paper Sereis*, 1990.

[11] Reinhard Latsch. Method for closed loop control of the instant of ignition. US, A, 4417556, Nov. 29 1983.

[12] James Lawton and Felix Weinberg. *Electrical Aspects of Combustion*. Oxford university press, 1969.

[13] J. Nytomt and T. Johansson. Metod och system för övervakning av förbränningsmotorer. SE, A, 95000189-7, 1995.

[14] J. D. Powell. Engine control using cylinder pressure: Past, present, and future. *Journal of Dynamic System, Measurement, and Control*, June 1993.

[15] H. R. Schwarz. *Numerical Analysis a Comprehensive Introduction*. John Whiley & Sons, 1989.

[16] Yuichi Shimasaki, Masaki Kanehiro, Shigeru Maruyama Shigeki Baba, Takashi Hisaki, and Shigeru Miyata. Spark plug voltage analysis for monitoring combustion in an internal combustion engine. *SAE Technical Paper Series*, 1993.

[17] United Electronic Industries, INC., Ten Dexter Avenue, Watertown, Massachusetts 02172 U.S.A. *User manual for: WIN-30*, second edition edition, December 1993.

Appendix A: A pre study on data from Mecel AB

An initial study was performed on data provided by Mecel AB. The study was performed on two different data sets from different engines. It is important to note that one data set in the pre study had a very clear post flame phase, and hence a relatively small flame front. During the prestudy, the ion peak and ion mass center algorithms were implemented and studied. The results from the pre study motivated further studies.

A.1   Characterization of the signals

The first data set is measured at four different operating points, and contains ten cycles each. The data for the operating points are shown in Table A.1. Some examples of the pressure and ionization signals are shown in Figures A.1 to A.3. These ionization signals have different characteristics from the data measured in the laboratory of Vehicular Systems. At the operating points with high load, the flame front is small compared to the post flame.

Operating point	1	2	3	4
Engine load	No load	WOT	No load	WOT
Engine speed	Idle	1200 rpm	5000 rpm	5000 rpm

Table A.1. Engine operating points for the data collected by Mecel AB. (WOT is wide open throttle.)
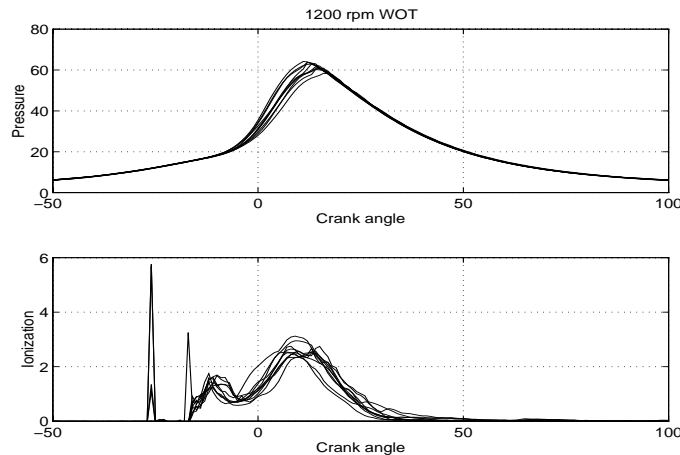

Figure A.1. Pressure and ionization current for 1200 rpm with wide open throttle.

The engine, on which these data sets were measured, has the spark plug mounted off-center near the combustion chamber wall. When the flame propagates through the combustion chamber it moves from the spark plug, where the ionization measurement is performed. Therefore there is a longer distance between the flame front in the combustion and the sensor. This distance might cause a lower signal level in the flame front phase. Another possible explanation is that the volume of the flame front is smaller when it propagates through the combustion chamber. The smaller flamfront might generate a smaller ionization signal.
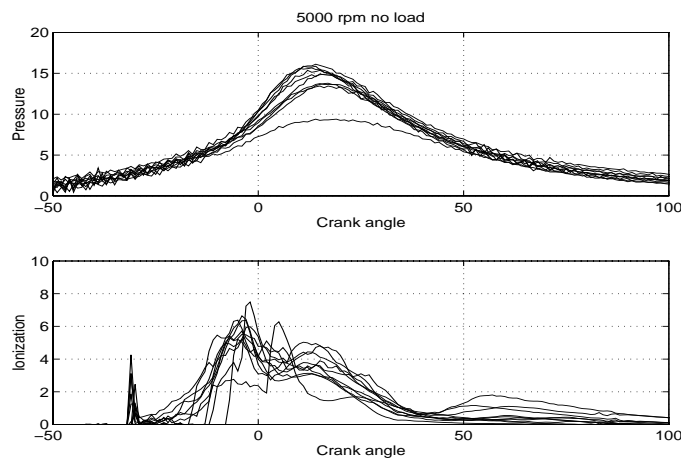
Figure A.2. Pressure and ionization current for 5000 *rpm* with no load.
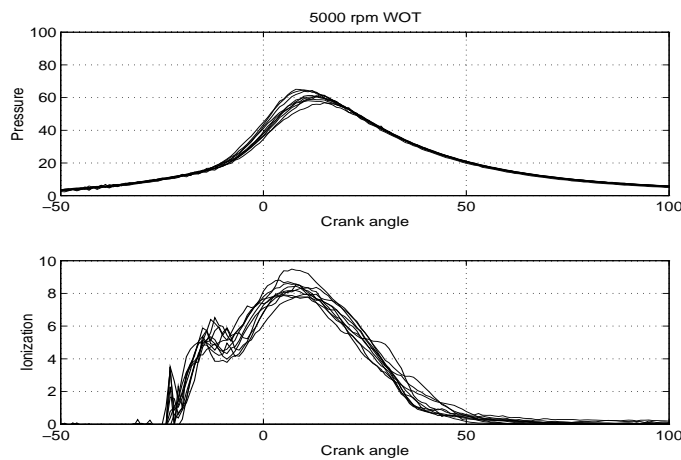

Figure A.3. Pressure and ionization current for 5000 *rpm* with wide open throttle.

The pressure for the data in the pre study has the same characteristics as the SAAB engine. Here the pressure peak appears at crank angles later than $7°$, this motivate the choice of a search start, mentioned in Section 5.2, of $5°$ after TDC for the ion peak algorithm.

The second data set, contained 500 cycles with only the ionization signal. The appearance of these data are similar to the data measured on the SAAB engine at Vehicular Systems. Therefore, it is not further presented. Since the data sets not contains the pressure signal, it was only used to verify the working principle of the mass center algorithm. More closely the choice of DP, Discarding Point, for the mass center algorithm was studied.

A.2 Algorithms

In the pre study the ion peak and ion mass center algorithms were tested. The algorithms are described in Section 5. Differences exist between the algorithms described there and the ones used in the pre study. The differences are mainly due to the different characteristics of the signals.

A search start is not necessary for the ion peak algorithm since the ionization signal has only one distinct peak, which appears in the flame front. The search in this study is made for crank angles between 10° before TDC and 30° after TDC. The signal is also smoothed before the search is made, where the smoothing filter is the same as described in Appendix B.

The ion structure analysis algorithm is not tested on the data in the pre study. The reason is that this algorithm was developed during the study of signals from the SAAB engine.

A.3   Results

For the operating point 6000 *rpm* and WOT, *Wide Open Throttle*, Figure A.4 show the position for the pressure peak and the points returned from the ion peak and ion mass center algorithms. The figure impose that the mass center for a signal that is cut-off
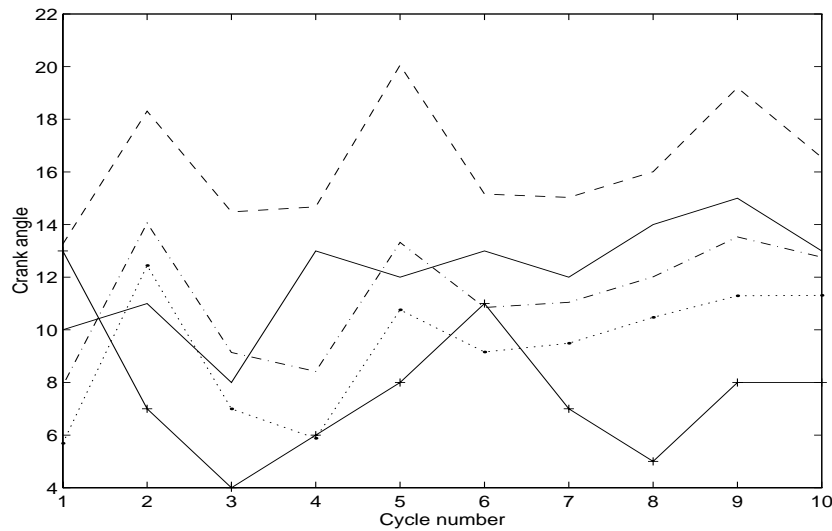

Figure A.4. The ionization mass centers, the pressure peak and the ion peaks. Filled line – pressure. Dashed line – Ion mass center with cut off. Dash dotted line – Correction with line. Dotted line – correction with parable. Filled line with + – Ion peak.
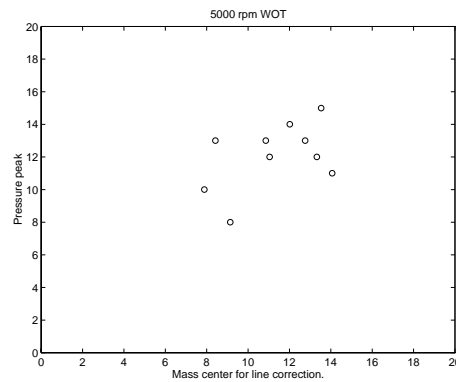

Figure A.5. Plot of the correlation between the ionization mass center, with a line as correction, and the pressure peak as well as the ion peak.

at DP, follows the pressure peak. It also imposes that the ion mass center follows the pressure peak better than the ion peak. The correlation plot between the peak pressure and the mass center algorithm with a line correction is shown in Figure A.5. In the figure a correlation is not visible since the dots are not placed on a straight line. Though, it must be noted that the data set contains only ten cycles, and it is dangerous to do statistics on such a small data set.

The results from the pre study motivated continued studies of the algorithms, for extracting information from the ionizaiton signal.

Appendix B: Smoothing filter

This section contains a description of the smoothing filter used in the ion peak and ion mass-center algorithms. The description contain the filter characteristics for both the time domain and frequency domain.

The demands on the filter are;

- It shall low pass filter the signal, removing the high frequency noise. This is in order to reduce the influence of noise on the first and second order derivatives.

- It shall not affect the phase of the filtered signal. This is in order to keep the time domain information of the ionization signal intact.

- The filter shall have gain = 1 for frequency 0.

The second demand is impossible to meet up with, if a causal filter is to be used. But since the whole signal is available during the filtering it is possible to use a non-causal filter, and therefore it it possible to meet this demand.

B.1   Time domain characteristic

No systematic design procedures have been used other than testing on ionization signals.

The filter is symmetric as is displayed in the equation

$$y(\theta_n) = a_0 u(\theta_n) + a_1(u(\theta_{n-1}) + u(\theta_{n+1})) + \cdots + a_N(u(\theta_{n-N}) + u(\theta_{n+N}))$$

The filter has the degree $2N + 1$, and it is non-causal since it use N forward values. Though, it is possible to rewrite this filter as a causal filter with a time delay of N samples and such a causal filter has linear phase characteristics. In order to achieve gain=1 at frequency 0, the sum of the filter coefficients must equal 1. This gives

$$a_0 + 2 \sum_{n=1}^{N} a_n = 1 \tag{B.1}$$

The filter coefficients used are

$$a_n = c \, \cos\left(\frac{\pi}{2}\frac{n}{N+1}\right)$$

where c is a constant, which make the coefficients fulfil (B.1).

B.2   Frequency domain characteristic

The impulse response for the filter is

$$h[n] = a_0\delta[n] + a_1\left(\delta[n+1] + \delta[n-1]\right) + a_2\left(\delta[n+2] + \delta[n-2]\right) + \cdots + a_N\left(\delta[n+N] + \delta[n-N]\right)$$

A Fourier transformation this gives the transfer function

$$H[\omega] = a_0 + a_1 2\cos(2\pi\omega) + a_2 2\cos(2\pi2\omega) + \cdots + a_N 2\cos(2\pi N\omega) \tag{B.2}$$

In figure B.1 the transfer function for the filter is displayed. The phase is not plotted since it is equal to zero. In the plot N is equal to 3 which gives the degree of the filter equal to 7. In a future implementation of the algorithms some more efforts can be put into designing the filter.
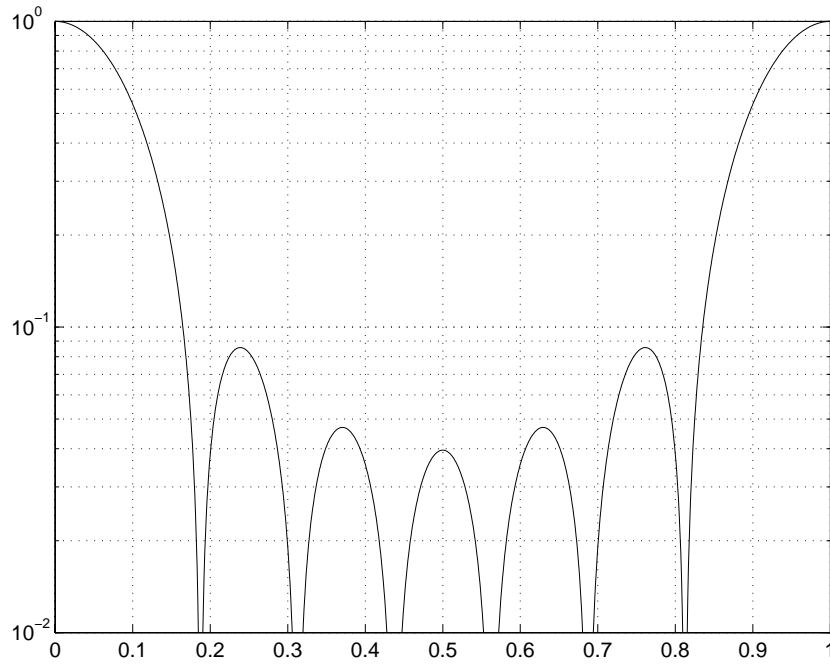
Figure B.1. Transfer function for the filter with degree 7.

B.3 Choice of degree

After some testing on the ionization signal, and studying the derivatives, the degree was chosen to 7. This gives the following filter

$$
\begin{aligned}
y(\theta_i) \quad = \quad & 0.199u(\theta_i) + 0.184(u(\theta_{i-1}) + u(\theta_{i+1})) \\
& + 0.140(u(\theta_{i-2}) + u(\theta_{i+2})) + 0.076(u(\theta_{i-3}) + u(\theta_{i+3}))
\end{aligned}
$$